

1 **Single cell transcriptome analysis reveals disease-defining T cell**
2 **subsets in the tumor microenvironment of classic Hodgkin lymphoma**

3
4 Tomohiro Aoki^{1,2,∞}, Lauren C. Chong^{1,∞}, Katsuyoshi Takata¹, Katy Milne^{3,4}, Monirath
5 Hav⁵, Anthony Colombo⁵, Elizabeth A. Chavez¹, Michael Nissen⁶, Xuehai Wang⁶,
6 Tomoko Miyata-Takata¹, Vivian Lam⁶, Elena Viganò^{1,2}, Bruce W. Woolcock¹, Adèle
7 Telenius¹, Michael Y. Li^{1,2}, Shannon Healy¹, Chanel Ghesquiere^{3,4}, Daniel Kos^{3,4}, Talia
8 Goodyear^{3,4}, Johanna Veldman⁷, Allen W. Zhang^{8,9}, Jubin Kim⁶, Saeed Saberi⁸, Jiarui
9 Ding^{8,10}, Pedro Farinha¹, Andrew P. Weng⁶, Kerry J. Savage¹, David W. Scott¹, Gerald
10 Krystal⁶, Brad H. Nelson^{3,11}, Anja Mottok^{1,12}, Akil Merchant⁵, Sohrab P. Shah^{2,8,9}, and
11 Christian Steidl^{1,2,*}

12
13 ¹ Centre for Lymphoid Cancer, British Columbia Cancer, Vancouver, BC, Canada

14 ² Department of Pathology and Laboratory Medicine, University of British Columbia,
15 Vancouver, BC, Canada

16 ³ Deeley Research Centre, British Columbia Cancer, Vancouver, BC, Canada

17 ⁴ Department of Biochemistry and Microbiology, University of Victoria, Victoria, BC,
18 Canada

19 ⁵ Cedars-Sinai Medical Center, Los Angeles, California, USA

20 ⁶ Terry Fox Laboratory, British Columbia Cancer, Vancouver, BC, Canada

21 ⁷ Department of Pathology and Medical Biology, University Medical Center Groningen,
22 University of Groningen, Groningen, The Netherlands

23 ⁸ Department of Molecular Oncology, British Columbia Cancer, Vancouver, BC,
24 Canada

25 ⁹ Department of Epidemiology and Biostatistics, Memorial Sloan Kettering Cancer
26 Center, New York, USA

27 ¹⁰ Broad Institute of MIT and Harvard, Cambridge, MA, USA

28 ¹¹ Department of Biochemistry and Microbiology, and Department of Biology,
29 University of Victoria, Victoria, BC, Canada

30 ¹² Institute of Human Genetics, Ulm University and Ulm University Medical Center,
31 Ulm, Germany

32 [∞] - equal contribution

33
34 ***Corresponding Author:**

35 Christian Steidl, MD

36 Centre for Lymphoid Cancer, British Columbia Cancer, Vancouver, BC, Canada

37 675 West 10th Ave, Room 12-110, Vancouver, BC V5Z 1L3, Canada

38 E-mail: CSteidl@bccancer.bc.ca

39 Phone (office): 604-675-8046

40 FAX:604-675-8183

41

42 **Running Title: Single cell characterization of Hodgkin lymphoma**

43

44 **Key words:** Hodgkin lymphoma, single-cell sequencing, immune biology, tumor

45 microenvironment, LAG3

46

47 **COMPETING INTERESTS**

48 C. Steidl reports receiving a commercial research grant from Bristol-Myers Squibb,

49 Trillium Therapeutics, and is a consultant/advisory board member for Seattle Genetics,

50 Curis, and Roche.

51

52

53

54

55

56

57 **ABSTRACT**

58 Hodgkin lymphoma (HL) is characterized by an extensively dominant tumor
59 microenvironment (TME) composed of different types of non-cancerous immune cells
60 with rare malignant cells. Characterization of the cellular components and their spatial
61 relationship is crucial to understanding crosstalk and therapeutic targeting in the TME.
62 We performed single-cell RNA sequencing of more than 127,000 cells from 22 HL
63 tissue specimens and 5 reactive lymph nodes, profiling for the first time the phenotype
64 of the HL-specific immune microenvironment at single-cell resolution. Single-cell
65 expression profiling identified a novel HL-associated subset of T cells with prominent
66 expression of the inhibitory receptor LAG3, and functional analyses established this
67 LAG3⁺ T cell population as a mediator of immunosuppression. Multiplexed spatial
68 assessment of immune cells in the microenvironment also revealed increased LAG3⁺ T
69 cells in the direct vicinity of MHC class-II deficient tumor cells. Our findings provide
70 novel insights into TME biology and suggest new approaches to immune checkpoint
71 targeting in HL.

72

73

74 **STATEMENT OF SIGNIFICANCE**

75 We provide detailed functional and spatial characteristics of immune cells in cHL at
76 single cell resolution. Specifically, we identified a Treg-like immunosuppressive subset
77 of LAG3⁺ T cells contributing to the immune escape phenotype. Our insights aid in the
78 development of novel biomarkers and combination treatment strategies targeting
79 immune checkpoints.

80

81

82

83

84

85

86

87

88

89

90

91

92 **INTRODUCTION**

93 Classic Hodgkin lymphoma (cHL) is the most common lymphoma subtype
94 among adolescents and young adults(1). cHL is characterized by an extensive
95 microenvironment composed of different types of non-cancerous normal immune cells,
96 such as several types of T cells, B cells, eosinophils and macrophages, and a rare
97 population (~1%) of clonal malignant Hodgkin and Reed-Sternberg (HRS) cells(1-3).
98 While some findings support the concept that the HRS cells recruit these immune cells
99 to form a tumor-supporting, regulatory tumor microenvironment (TME) with limited
100 anti-tumor activity in cHL(4-6), the complex interactions between HRS cells and their
101 TME remain only partially understood. A deeper understanding of this symbiotic
102 cellular crosstalk ('ecosystem') may lead to the development of novel biomarkers and
103 therapeutic approaches.

104 Immune checkpoint inhibitors, such as the programmed death 1 (PD-1)
105 inhibitors nivolumab and pembrolizumab, have shown dramatic efficacy in relapsed or
106 refractory cHL with an overall response rate (ORR) of 65-87%(7,8), and durable
107 remissions of approximately 1.5 years(8), which compares very favorably to other
108 agents in this setting(9). Although the emergence of novel drugs emphasizes the need
109 for the identification of predictive biomarkers that can provide a rationale for treatment

110 selection, it remains unclear which cells are the most important targets of immune
111 checkpoint inhibitors and which components are most relevant for the immune escape
112 phenotype in cHL. Thus, further comprehensive investigations of this interaction are
113 needed.

114 Previous studies have applied immunohistochemistry (IHC), microarray,
115 cytometry by time-of-flight (CyTOF) and NanoString assays to characterize the
116 immune phenotype of the TME in cHL, and have identified some important associations
117 between the presence of certain immune cell types and clinical outcome(4,6,10).

118 Although previous reports have described enrichment of CD4⁺ T cells in the TME of
119 cHL(10-12), their study scale has been limited and detailed co-expression patterns of
120 important markers such as inhibitory receptors have not been examined.

121 Recently, the landscape of tumor infiltrating T cells has been assessed using
122 single-cell transcriptome sequencing in several solid tumors, mostly of epithelial
123 origin(13,14). These single-cell RNA sequencing (scRNA-seq) studies have revealed
124 diverse immune phenotypes, such as cells exhibiting an exhaustion signature, as well as
125 clonal expansion patterns of T cell lineages(14). However, such analyses are currently
126 lacking in lymphomas, which differ from most solid cancers in that they are clonally
127 derived from lymphocytes that professionally interact with other immune cells in the

128 ecosystem of the microenvironment.

129 In this study, we performed high dimensional and spatial profiling of immune
130 cells in cHL using scRNA-seq of 127,786 cells, multicolor IHC and imaging mass
131 cytometry (IMC). We identified unique regulatory T cell-like subset that expressed
132 lymphocyte activation gene 3 (LAG3⁺ T cells) in cHL and were mostly absent in normal
133 reactive lymph nodes. LAG3⁺ T cells were characterized by expression of
134 interleukin-10 (IL-10) and transforming growth factor β (TGF- β), and we demonstrated
135 an immuno-suppressive function of these cells. Further topological analysis revealed
136 that HRS cells were closely surrounded by frequent LAG3⁺ T cells in the subset of cHL
137 patients with loss of Major histocompatibility class II (MHC-II) expression on tumor
138 cells. Our data provide an unprecedented number of single-cell transcriptomes in
139 combination with multiplexed spatial assessment, allowing us to decipher the unique
140 immune cell architecture of the TME in cHL with implications for novel therapies,
141 including rational combinations and predictive biomarker development.

142

143

144

145 **RESULTS**

146 **The cHL-specific immune microenvironment at single-cell resolution**

147 To characterize the transcriptional profile of immune cells in the TME of cHL,
148 we performed scRNA-seq on single cell suspensions collected from lymph nodes of 22
149 cHL patients, including 12 of nodular sclerosis (NS) subtype, 9 of mixed cellularity
150 (MC) subtype, and 1 of lymphocyte-rich (LR) subtype. We also sequenced reactive
151 lymph nodes (RLN; $n = 5$) from healthy donors as normal controls (**Supplementary**
152 **Tables 1 and 2**). Transcriptome data were obtained for a total of 127,786 sorted live
153 cells, with a median of 1,203 genes detected per cell (**Supplementary Table 3**). To
154 perform a systematic comparative analysis of the cHL TME and RLN, we merged the
155 expression data from all cells (cHL and RLN) and performed batch correction and
156 normalization. Removal of batch effects (caused by single cell isolation and library
157 preparation in different experimental runs) resulted in improved mixing of cells across
158 samples, as demonstrated by a significant increase in cell entropy
159 (Wilcoxon-Mann-Whitney $p < 0.001$; **Supplementary Fig. 1A-B**).

160 Unsupervised clustering using PhenoGraph followed by visualization in t-SNE
161 space(15,16) identified 22 expression-based cell clusters that were annotated and
162 assigned to a cell type based on the expression of genes described in published

163 transcriptome data of sorted immune cells(17) and known canonical markers (**Fig. 1A**;
164 **Supplementary Fig. 2A-E and 3**). These included 4 naïve T cell clusters, 2 CD8⁺ T
165 cell clusters, 6 CD4⁺ T cell clusters, 7 B cell clusters, 1 macrophage cluster, 1
166 plasmacytoid dendric cell cluster and 1 progenitor cell cluster. We could not observe
167 HRS cell cluster may be due to limitation of microfluidics approach. While most
168 immune cell phenotypes exhibited overlap between cHL and RLN as demonstrated by
169 clusters containing a mixture of cell types, we observed an enrichment of cells from
170 cHL in some specific cell clusters (**Fig. 1B**). Of interest, we found that all three
171 regulatory T cell (Treg) clusters were quantitatively dominated by cells derived from the
172 cHL samples with only a minor proportion originating from RLNs (**Fig. 1C**), and that
173 the proportion of cells assigned to Treg clusters was significantly higher in cHL samples
174 compared to RLN (P = 0.0001; t-test; **Fig. 1D**). The cluster containing the highest
175 proportion of immune cells from cHL samples (“CD4-C5-Treg”) also exhibited
176 relatively high expression of LAG3 and CTLA4 (**Fig. 1A**). Conversely, clusters
177 enriched in RLN were mostly B cell and CD8⁺ T cell clusters (**Fig. 1C**). Further
178 examination of the non-Treg CD4⁺ T cell clusters revealed that they were primarily
179 composed of type 2 T helper (Th2) cells, and that Th1 and Type 17 T helper (Th17)
180 cells were also enriched in cHL samples compared to RLN (**Fig. 1E**). We also

181 performed differential expression analysis between cHL and RLN cells within each
182 cluster, and identified IL-32 as consistently upregulated in cHL T cells compared to
183 RLN T cells (**Supplementary Fig. 4**). IL-32 is a known pro-inflammatory cytokine that
184 can induce the production of other cytokines such as IL-6(18).

185

186 **EBV status affects the immune cell subset composition in cHL**

187 Thirty to 40% of cHL are associated with latent Epstein-Barr virus (EBV)
188 infection of the malignant HRS cells(19), and several reports indicate that EBV
189 infection can recruit specific Treg populations to the TME in cHL(20,21). To more
190 precisely define immune cell composition according to EBV status, we compared the
191 RNA-seq data of 5 EBV⁺ vs 17 EBV⁻ cases (**Supplementary Fig. 5A**). The proportion
192 of CD4⁺ T cells with a Th17 profile was significantly decreased in EBV⁺ cHL (P =
193 0.004; t-test) (**Fig. 1F-G**). However, there was no significant difference between EBV⁺
194 and EBV⁻ cases with respect to CD8⁺ T cell or Treg proportions (**Fig. 1F;**
195 **Supplementary Fig. 5B**). Similarly, the cHL mixed cellularity (MC) subtype, which is
196 more commonly associated with EBV related cHL, was associated with a lower
197 proportion of Th17 polarized immune cells as compared to the nodular sclerosis (NS)
198 subtype (**Fig. 1H; Supplementary Fig. 5C**).

199

200 **Single cell expression patterns of novel cHL-specific immune subsets**

201 Our data demonstrated the preferential enrichment of Tregs in cHL as compared
202 to RLN (**Fig. 1B and D**). Considering the importance of an immuno-suppressive
203 microenvironment as a cancer hallmark, and its implications for biomarker development
204 and targeted immunotherapy, we focused our analyses on the detailed characterization
205 of Treg subsets. The most cHL-enriched Treg cluster, CD4-C5-Treg (**Fig. 1A**), was
206 characterized by high expression of LAG3 in addition to common Treg markers such as
207 IL2RA (CD25) and TNFRSF18 (GITR) (**Fig. 2A**). However, other canonical Treg
208 markers such as FOXP3 were not co-expressed in this cluster, suggesting these cells
209 may exhibit a type 1 regulatory (Tr1) T cell phenotype(20,22) (**Fig. 2B;**
210 **Supplementary Fig. 6A**). To confirm the expression pattern of immune cells in cHL,
211 we also assessed the expression of surface and intracellular markers in all cHL cases
212 using multi-color IHC and IMC. The orthogonal data confirmed the inversely correlated
213 expression pattern of LAG3 and FOXP3 on CD4⁺ T cells at the protein level
214 (**Supplementary Fig. 6B-C**).

215 Inhibitory receptor-mediated immune tolerance that can be hijacked by tumors
216 has been a major target of cancer immunotherapy(23,24). To gain more insight into the

11

217 characteristics of inhibitory receptor expression in the TME of cHL, we explored
218 expression patterns among individual T cells. While LAG3-expressing cells were
219 mostly assigned to Treg clusters, PD-1-expressing cells were primarily assigned to
220 non-Treg CD4⁺ T cell clusters (**Fig. 2C**). Interestingly, CD8⁺ T cells, including CTLs,
221 are not the dominant population expressing PD-1 and LAG3 (**Fig. 2C-D**), indicating the
222 importance of the CD4⁺ T cell population for immune checkpoint regulation in cHL.
223 Notably, the expression pattern of inhibitory receptors was variable among T cell
224 subsets (**Fig. 2E**), suggesting a specific role of each inhibitory receptor in each T cell
225 subset in cHL. Analyzing co-expression patterns on the single cell level revealed that
226 the majority of LAG3⁺ T cells co-expressed CTLA4 which is known as more universal
227 Treg marker, but not PD-1 (**Fig. 2F**). Similarly, most PD-1⁺ T cells did not co-express
228 LAG3. CTLA-4 was also co-expressed by FOXP3⁺ T cells (**Supplementary Fig. 6A**).
229 These co-expression patterns were validated using FCM (**Supplementary Fig. 7A-B**).
230 Interestingly, LAG3, TIGIT and PD-1 were not co-expressed by the majority of CD8⁺ T
231 cells. Furthermore, although we observed a trend towards higher proportions of
232 non-TFH (Follicular helper T) PD-1⁺ CD4⁺ T cells in RLN samples, the proportion of
233 LAG3⁺ cells was significantly higher in cHL, suggesting a unique role of LAG3⁺ CD4⁺
234 T cells in cHL pathogenesis (**Supplementary Fig. 7C**).

235 To explore the functional role of LAG3⁺ T cells, we next applied the diffusion
236 map algorithm(25,26) with the aim of characterizing differentiation states among CD4⁺
237 T cells (**Fig. 2G**). Most T cells were grouped by PhenoGraph cluster, and the first
238 dimension showed a trajectory beginning with naïve T cells and ending with Tregs.
239 LAG3⁺ T cells were enriched at the far end of this dimension, which was correlated with
240 genes representative of a terminal differentiation signature (**Methods; Supplementary**
241 **Fig. 8A**). Consistent with a previous report that showed LAG3⁺ T cells confer
242 suppressive activity through their significantly reduced proliferation activity(27),
243 LAG3⁺ T cells were also located in the middle to negative end of the second dimension,
244 which correlated with G2/M cell cycle and glycolysis signature genes (**Supplementary**
245 **Fig. 8B**). Furthermore, the most positively correlated genes with dimension 1 were
246 LAG3, LGMN and CTLA4, which are known markers of suppressive function in Tregs,
247 indicating the suppressive signature of LAG3 in these T cells (**Supplementary Fig.**
248 **8C-D**).

249

250 **cHL cell line supernatant can induce LAG3⁺ T cells**

251 To characterize the immunosuppressive signature of Tregs in cHL, we
252 investigated the cytokine expression of LAG3⁺ T cells. Among the CD4⁺ cluster T cells,

253 LAG3⁺ T cells had higher expression of immune-suppressive cytokines IL-10, TGF- β
254 and IFN- γ compared to LAG3⁻ T cells (**Fig. 3A**). These characteristics are consistent
255 with the profile of type 1 regulatory T cells(28,29).

256 Taken together, our data consistently demonstrate a suppressive phenotype of
257 LAG3⁺ T cells in cHL. We hypothesized that cytokines or chemokines produced by
258 HRS cells might influence the TME in cHL. Thus, we next assessed the effect of
259 supernatant transfer of various lymphoma cell lines on the expansion of T cells *in vitro*.
260 After 14 days of activation of T cells, flow cytometry analysis confirmed that CD4⁺
261 CD25⁺ T cells co-cultured with cHL cell line supernatant expressed significantly higher
262 levels of LAG3 as compared to those co-cultured with diffuse large B-cell lymphoma
263 (DLBCL) cell line supernatant or medium only (**Fig. 3B-C**). Luminex analysis revealed
264 that the presence of cHL cell line supernatant resulted in enrichment of multiple
265 cytokines and chemokines as compared to DLBCL cell lines, including TARC/CCL17,
266 TGF- β , and IL-6, which are known enhancers of Treg migration and
267 differentiation(30-38) (**Fig. 3D**). Consistent with scRNA-seq results, CD4⁺ LAG3⁺ T
268 cells isolated by FACS secreted significantly higher amounts of IL-10 and
269 TGF- β compared to CD4⁺ LAG3⁻ T cells (**Fig. 3E**). Notably, CD4⁺ LAG3⁺ T cells
270 suppressed the proliferation of responder CD4⁺ T cells when co-cultured *in vitro*,

271 confirming an immunosuppressive function of the LAG3⁺ T cells (**Fig. 3F**).

272

273 **Spatial assessment of LAG3⁺ T cells and HRS cells**

274 We next sought to understand the spatial relationship between LAG3⁺ T cells
275 and malignant HRS cells. IHC of all cases revealed that LAG3⁺ T cells were enriched in
276 the cHL TME compared to RLN, and in a subset of cHL cases HRS cells were closely
277 surrounded by LAG3⁺ T cells (**Fig. 4A**). Of note, our single cell analysis revealed that
278 LAG3 expression was significantly higher in cases with MHC class II negative HRS
279 cells (n = 6) as compared to those with MHC class II positive cHL cases (n = 16), but
280 was not correlated with EBV status or histological subtype (**Fig. 4B; Supplementary**
281 **Fig. 9A-C**). Strikingly, when examining cells within the CD4-C5-Treg cluster, LAG3
282 was identified as the most up-regulated gene in MHC class II negative cells compared
283 to MHC class II positive cells (**Fig. 4C**). Characterization of immune markers using
284 IHC showed not only a marked increase in LAG3⁺ T cells, but also a decrease in
285 FOXP3⁺ T cells in MHC-II negative cases when compared to MHC-II positive cases
286 (**Fig. 4D**). There was no difference in the proportion of CTLA4⁺ CD4⁺ T cells by
287 MHC-II status, suggesting the LAG3⁺ cells represent a distinct sub-population of the
288 HL-specific CTLA4⁺ cells previously reported(12) (**Supplementary Figure 9D**). To

289 validate these findings, we assessed the spatial relationship between HRS cells and
290 LAG3⁺ CD4⁺ T cells using multicolor IHC (**Fig. 4E-G**). We confirmed that the density
291 of LAG3⁺ T cells in HRS-surrounding regions was significantly increased in MHC class
292 II negative cases, but not correlated with either MHC class I status, pathological subtype
293 or EBV status (**Fig. 4E; Supplementary Fig. 10A**). Similarly, the average nearest
294 neighbor distance between CD30⁺ cells (HRS cells) and their closest LAG3⁺ T cell was
295 significantly shorter in MHC class II negative cHL cases (**Fig. 4F**). In contrast, the
296 density of HRS-surrounding FOXP3⁺ T cells was higher in cases with MHC class II
297 positive HRS cells (**Fig. 4E; Supplementary Fig. 10B**), and the nearest neighbor
298 distance from HRS cells to FOXP3⁺ cells was also shorter in these cases (**Fig. 4F;**
299 **Supplementary Fig. 11A-B**).

300 To further investigate the spatial relationship between HRS cells and their
301 surrounding cells, we next assessed the expression of surface and intracellular markers
302 in all cHL study cases using IMC, which allows for simultaneous interrogation and
303 visualization of 35 protein markers in the spatial context of the TME. Consistent with
304 IHC analysis, IMC revealed that MHC class II negative cHL cases showed numerous
305 LAG3⁺ CD4⁺ cells, with rare FOXP3⁺ CD4⁺ cells (**Fig. 5A; Supplementary Fig. 12A**).
306 In contrast, MHC class II positive cases showed rare LAG3⁺ CD4⁺ T cells and abundant

307 FOXP3⁺ CD4⁺ T cells rosetting the HRS cells. We also confirmed the observed
308 significantly shorter nearest neighbor distances between HRS cells and their closest
309 LAG3⁺ T cell in MHC class II negative cHL cases when compared to MHC class II
310 positive cHL cases using IMC data (**Supplementary Fig. 12B-C**).

311

312 **The number of LAG3⁺ T cells in the tumor microenvironment is correlated with**
313 **loss of MHC-II expression in a large validation cohort**

314 We next validated our findings using IHC of an independent cohort of 166
315 patients uniformly treated with first-line ABVD (doxorubicin, bleomycin, vinblastine
316 and dacarbazine) as described in Steidl et al(6) and investigated the potential prognostic
317 value of the presence of LAG3⁺ T cells. Consistent with the results from scRNA-seq,
318 we found that the proportion of LAG3⁺ T cells present in tumor tissue was significantly
319 higher in cases with MHC class II negative HRS cells as compared to those with MHC
320 class II positive HRS cells, but was not associated with EBV status (**Fig. 5B-C**). In
321 addition, we observed a trend towards shortened disease-specific survival (DSS; P =
322 0.072) and overall survival (OS; P = 0.12) in patients with an increased number of
323 LAG3⁺ T cells (**Supplementary Fig. 13A-B**). Of note, a high proportion of LAG3⁺ T
324 cells (> 15%) and CD68⁺ tumor-associated macrophages (≥ 5%)(6) were identified as

325 independent prognostic factors for DSS by multivariate Cox regression analysis (also
326 considering MHC II expression and International Prognostic Score (IPS) as variables;
327 **(Supplementary Fig. 13C)**). In the absence of statistically significant outcome
328 correlates in the present cohorts of pretreatment HL samples, we examined an
329 independent cohort of patients with relapsed cHL uniformly treated with high dose
330 chemotherapy followed by autologous stem cell transplantation (ASCT)(4). We
331 similarly found that abundant LAG3⁺ T cells were associated with unfavorable
332 post-ASCT survival, although statistical significance was not reached, likely due to
333 sample size **(Supplementary Fig. 13D)**.

334

335 **Cross-talk between HRS cells and LAG3⁺ T cells in cHL**

336 To investigate the role of HRS cells in their interaction with the cHL
337 microenvironment, we next explored Affymetrix gene expression data generated from
338 micro-dissected HRS cells of primary HL samples(39) (see **Supplementary Methods**
339 for details). We validated the high expression level of the cytokines and chemokines
340 that we observed in the *in vitro* Luminex assay (**Fig. 6A**). Notably, IL-6, which is a
341 known promoter of Tr1 cell differentiation(38), was the only cytokine that showed
342 significantly higher expression in MHC-II negative HRS cells compared to MHC-II

343 positive HRS cells. CD4⁺LAG3⁺ T cells were also induced by IL-6 *in vitro* (**Fig. 6B**),
344 indicating that IL-6 might play a role in inducing CD4⁺LAG3⁺ T cells in cHL.

345 MHC-II is also a known LAG-3 ligand(40,41). To investigate the interaction
346 between LAG3⁺ T cells and MHC-II on HRS cells, we generated *CIITA* knockouts in
347 the L-428 cHL cell line, as *CIITA* is the master regulator of MHC-II expression, and
348 confirmed the MHC-II negative status of these *CIITA* knockout cells (**Supplementary**
349 **Fig. 14A**). Next, we isolated LAG3⁺ T cells induced from PBMC using L-428
350 supernatant transfer. In co-culture of these LAG3⁺ T cells with either *CIITA* wild-type
351 or knockout L-428 cells, we observed that LAG-3 expression was significantly
352 decreased with MHC-II positive L-428, suggesting negative regulation of LAG3⁺ T cell
353 function through a direct MHC-II-LAG3 interaction (**Fig. 6C**). We also evaluated
354 expression of cytokines, including IL-6 and TARC, from both *CIITA* wild-type and
355 knockout L-428 cells, and observed no significant difference (**Supplementary Fig.**
356 **14B**). Taken together, these findings suggest that while IL-6 induces LAG3⁺ T cells,
357 MHC-II positivity actively depletes them, thus a mechanism for induction and
358 persistence is present only in MHC-II negative tumors. We also investigated the
359 expression of other LAG3 ligands on HRS cells according to MHC-II status in the
360 Affymetrix dataset, and found that their expression was not significantly increased

361 relative to normal GCB cells (**Supplementary Fig. 14C**). In addition, there was no
362 correlation between the expression level of LAG3 ligands according to MHC-II status,
363 suggesting no direct interaction with these ligands in cHL.

364

365 **T cells from cHL clinical samples are activated after removal of LAG3⁺ T cells**

366 To confirm the pathogenic role of LAG3⁺ T cells in cHL clinical samples, we
367 sorted both CD4⁺ LAG3⁺ CD25⁺ T cells and remaining T cells from cell suspensions of
368 4 patients. We then co-cultured T cells with or without CD4⁺ LAG3⁺ CD25⁺ T cells *in*
369 *vitro*, and observed that proliferation was suppressed in the T cells co-cultured with the
370 LAG3⁺ population, while proliferation and expression of the intracellular cytokine,
371 TNF α , were significantly increased in the population cultured without LAG3⁺ cells (**Fig.**
372 **6D-E, Supplementary Fig. 15**). These results support an immunosuppressive function
373 of CD4⁺ LAG3⁺ T cells in cHL clinical samples, providing preclinical rationale for
374 targeting LAG3⁺ T cells and their interactions to promote reactivation of T cells in a
375 subset of patients.

376 Our results suggest a model in which the immunosuppressive
377 microenvironment of MHC class II negative HRS cells (Type 1) is highly organized and
378 in part induced by CD4⁺ LAG3⁺ T cells, which in turn are induced by cytokines and

379 chemokines produced by HRS cells (**Fig. 7**). Aggregating all of these results, we reason
380 that cross-talk between LAG3⁺ T cells and HRS cells may be an essential mechanism of
381 immune escape in cHL, with potential implications for outcome prediction of
382 differential checkpoint inhibitor therapy including response durability and overcoming
383 resistance.

384

385 **DISCUSSION**

386 Using scRNA-seq and IMC at an unprecedented scale, we comprehensively
387 characterized immune cell populations to generate an immune cell atlas of the TME in
388 classic Hodgkin lymphoma at both the RNA and protein level. In addition to
389 reproducing known TME characteristics in cHL at single cell resolution, such as a
390 Treg/Th2-rich environment(10,11), a Th17-predominant profile in EBV⁺ cHL(42), and
391 a CTLA-4⁺ PD1⁻ T cell population(12), we also identified and characterized in detail
392 novel cellular subpopulations, including immuno-suppressive LAG3⁺ T cells(40) that
393 are linked to unique pathologic and clinical parameters. Strikingly, Treg populations
394 and the LAG3⁺ T cell population in particular emerged as the most highly enriched and
395 cHL-characteristic cellular component.

396 LAG3 is a selective marker of type 1 T regulatory (Tr1) cells, which in contrast to

397 natural Tregs derived from the thymus, are known as induced Tregs that exhibit strong
398 immunosuppressive activity(20-22,27). Consistent with characteristics of Tr1 cells, the
399 expression of the suppressive cytokines IL-10 and TGF- β (22,27), was very high in
400 LAG3⁺ T cells, whereas FOXP3 was not co-expressed in LAG3⁺ T cells in our
401 scRNA-seq and IMC data. Furthermore, LAG3⁺ T cells demonstrated substantial
402 suppressive activity *in vitro*, indicating an immunosuppressive role of these cells in the
403 TME of cHL.

404 Unlike previous reports that found EBV infection increased Tr1-related gene
405 expression including LAG3 in cHL(20), we identified a significant LAG3⁺ Treg
406 population regardless of EBV status by scRNA-seq, multi-color IHC, IMC, and single
407 color IHC analyses in independent cohorts. However, our study revealed that LAG3⁺
408 CD4⁺ T cells were enriched in cases with MHC class II negative HRS cells.
409 Interestingly, MHC class II deficiency was reported as a predictor of unfavorable
410 outcome after PD-1 blockade(43). Our scRNA-seq data revealed that each T cell subset
411 had a specific expression pattern of inhibitory receptors including PD-1 and LAG3.
412 Most notably, the majority of LAG3⁺ CD4⁺ T cells did not co-express PD-1, and the
413 absence of PD-1 has been reported to represent functionally active Tregs in solid
414 cancer(44), indicating the potential of LAG3 as a separate and complementary

415 immunotherapeutic target in cHL. The FOXP3⁺ Tregs that are enriched in MHC-II
416 positive HRS cells in this study might be similar to the PD-1 negative FOXP3⁺ Tregs
417 previously reported(10).

418 MHC class II is one of the major ligands of LAG3(40,41) and we showed
419 negative regulation of LAG3⁺ T cell expression through MHC-II and LAG3 interaction
420 using HL cell lines *in vitro*. These results are consistent with the patient data showing
421 that LAG3⁺ CD4⁺ T cells were preferentially observed surrounding MHC class II
422 negative HRS cells. Additionally, our *in vitro* co-culture findings suggest that cytokines
423 and chemokines produced by HRS cells may be an important inducer of LAG3⁺ CD4⁺ T
424 cells in the TME. In particular, re-analysis of expression on laser micro-dissected HRS
425 cells revealed that MHC-II negative HRS cells had higher levels of IL-6, a cytokine
426 known to induce Tr1 cells(38). Alternative ligands of LAG3 that mediate the immune
427 suppressive function(45,46) might contribute to these interactions, although we did not
428 observe any differences in their expression on HRS cells according to MHC-II status.

429 Our findings suggest that LAG3⁺ T cells induced by cytokines and chemokines
430 from HRS cells play an important role in substantial immunosuppressive activity in the
431 TME of cHL. Importantly, LAG3 is a cancer immuno-therapeutic target in ongoing
432 clinical trials in malignant lymphoma, including cHL (NCI trial ID 02061761), and we

433 showed the potential of removing the LAG3⁺ population as a means of reactivating T
434 cell activity. While currently our data do not demonstrate value of LAG3⁺ T cells as a
435 *prognostic* biomarker, and pending further studies in additional cohorts, it will be
436 critical to evaluate the potential of LAG3⁺ T cells as a *predictive* biomarker in the
437 context of treatments targeting LAG3⁺ T cells and their cellular interactions. In
438 particular, ongoing trials of LAG3-targeting antibodies and antibody-drug conjugates
439 against CTLA-4 or CD25 (which would target LAG3⁺ cells among others) will allow
440 this evaluation. Moreover, additional investigations into the biology of immune cell
441 interactions, including LAG3⁺ T cells and other immune cell types, may be beneficial
442 for future therapeutic development of alternative checkpoint inhibitors.

443 In conclusion, our comprehensive analysis provides, for the first time, detailed
444 functional and spatial characteristics of immune cells in the cHL microenvironment at
445 single cell resolution. We identified unique expression signatures of TME cells,
446 including LAG3⁺ T cells, and our findings provide novel insights and texture to the
447 central hypothesis of CD4⁺ T cell mediated immune-suppressive activity in the
448 pathogenesis of cHL. Importantly, our findings will facilitate a deeper understanding of
449 the mechanisms underlying the immune escape phenotype in cHL, and aid in the
450 development of novel biomarkers and treatment strategies.

451 **METHODS**

452 Detailed materials and methods are available in the Supplementary Data file.

453

454 **Tissue samples**

455 For single cell RNA sequencing, a total of 22 patients with histologically confirmed
456 diagnostic (n = 21) or relapsed (n = 1) classic Hodgkin Lymphoma (cHL) and reactive
457 lymphoid hyperplasia (but no evidence of malignant disease or systemic autoimmune
458 disease) (n = 5) were included in this study. Patients were selected based on the
459 availability of tissue that had been mechanically dissociated and cryopreserved as cell
460 suspensions following diagnostic lymph node biopsy from British Columbia (BC)
461 Cancer. Patient characteristics are summarized in Supplementary Table 1 and 2.

462 The independent validation cohort consisted of 166 cHL patients uniformly treated
463 with ABVD at BC Cancer between 1994 and 2007 from the cohort described in Steidl et
464 al(6). This cohort was derived from a population-based registry (Centre for Lymphoid
465 Cancer database, BC Cancer Agency), enriched for treatment failure. The median
466 follow-up time for living patients was 4.1 years (range: 0.5 to 24.4 years). The relapse
467 cohort consisted of 55 relapsed or refractory cHL patients uniformly treated with high
468 dose chemotherapy and ASCT at BC Cancer, from the cohort described in Chan et

469 al(4).

470 This study was reviewed and approved by the University of British Columbia-BC
471 Cancer Agency Research Ethics Board (H14-02304), in accordance with the
472 Declaration of Helsinki. We obtained written informed consent from the patients or the
473 need for consent was waived in the retrospective study.

474

475 **Single cell RNA sequencing sample preparation**

476 To identify live cells, we used DAPI (Sigma-Aldrich, St. Louis, MO) for live-dead
477 discrimination. Cell suspensions from cHL tumors or reactive lymph node were rapidly
478 defrosted at 37°C, washed in 10ml of RPMI1640/10% fetal bovine serum (FBS)
479 solution or RPMI1640/20% FBS solution containing DNase I (Millipore Sigma,
480 Darmstadt, Germany) and washed in PBS. Cells were resuspended in PBC containing
481 3% FBS and stained with DAPI for 15 min at 4°C in the dark. Viable cells (DAPI
482 negative) were sorted on a FACS ARIAIII or FACS Fusion (BD Biosciences) using an
483 85 µm nozzle (**Supplementary Fig. 16**). Sorted cells were collected in 0.5 ml of
484 medium, centrifuged and diluted in 1x PBS with 0.04% bovine serum albumin (BSA).
485 Cell number was determined using a Countess II Automated Cell Counter whenever
486 possible.

487

488 **Library Preparation and single-cell RNA sequencing**

489 In total, 8,600 cells per sample were loaded into a Chromium Single Cell 3' Chip kit v2

490 (PN-120236) and processed according to the Chromium Single Cell 3' Reagent kit v2

491 User Guide. Libraries were constructed using the Single 3' Library and Gel Bead Kit v2

492 (PN-120237) and Chromium i7 Multiplex Kit v2 (PN-120236). Single cell libraries

493 from two samples were pooled and sequenced on one HiSeq 2500 125 base PET lane.

494 CellRanger software (v2.1.0; 10X Genomics) was used to demultiplex the raw data,

495 generate quality metrics, and generate per-gene count data for each cell.

496

497 **Normalization and batch correction**

498 Analysis and visualization of scRNA-seq data was performed in the R statistical

499 environment (v3.5.0). CellRanger count data from all cells ($n = 131,151$) were read into

500 a single 'SingleCellExperiment' object. Cells were filtered if they had $\geq 20\%$ reads

501 aligning to mitochondrial genes, or if their total number of detected genes was ≥ 3

502 median absolute deviations from the sample median. This yielded a total of 127,786

503 cells for analysis. The scran package (v1.9.11) was used to quick cluster the cells and

504 compute cell-specific sum factors with the method described by Lun et al(47). (see

27

505 **Supplementary Methods** for details). The scater package (v1.8.0) was used to

506 log-normalize the count data using the cell-specific sum factors.

507 To remove batch effects resulting from different chips and library preparation,

508 the fast mutual nearest neighbors (MNN) batch correction technique in the scan

509 package was utilized, grouping cells by their chip and using the expression of genes

510 with positive biological components (see **Supplementary Methods** for details). This

511 produced a matrix of corrected low-dimensional component coordinates ($d = 50$) for

512 each cell, which was used as input for downstream analyses. Entropy of cell expression

513 before and after batch correction was assessed in R using the method described by Azizi

514 et al(13) (**Supplementary Fig. 1B; Supplementary Methods**).

515

516 **Clustering and annotation**

517 Unsupervised clustering was performed with the PhenoGraph algorithm(48), using the

518 first 10 MNN-corrected components as input. Clusters from PhenoGraph were manually

519 assigned to a cell type by comparing the mean expression of known markers across cells

520 in a cluster (see **Supplementary Methods** for details). For visualization purposes, tSNE

521 transformation was performed with the scater package using the first 10 MNN-corrected

522 components as input. All differential expression results were generated using the

523 *findMarkers* function of the *scran* package, which performs gene-wise t-tests between
524 pairs of clusters, and adjusts for multiple testing with the Benjamini-Hochberg method.
525 Diffusion map analysis(25) was performed using the algorithm implemented by the
526 *scater* package (**Supplementary Methods**).

527

528 **Multi-color IHC on TMA, scanning and image analysis**

529 TMA slides were deparaffinized and incubated with each marker of interest (MHC class
530 II, FOXP3, CD8, LAG3, CD4, CD30), followed by detection using Mach2 HRP and
531 visualization using Opal fluorophores (**Supplementary Table 4**; see **Supplementary**
532 **Methods** for details). Nuclei were visualized with DAPI staining. TMA slides were
533 scanned using the Vectra multispectral imaging system (PerkinElmer, USA) following
534 manufacturer's instructions to generate .im3 image cubes for downstream analysis. To
535 analyze the spectra for all fluorophores included, inForm image analysis software
536 (v2.4.4; PerkinElmer, USA) was used. Cells were first classified into tissue categories
537 using DAPI and CD30 to identify CD30⁺ DAPI⁺, CD30⁻ DAPI⁺, and CD30⁻ DAPI⁻ areas
538 via manual circling and training (**Supplementary Fig. 17**). The CD30⁺ DAPI⁺ regions
539 were considered to be HRS-surrounding regions. Cells were then phenotyped as

540 positive or negative for each of the six markers (MHC class II, FOXP3, CD8, LAG3,
541 CD4, CD30). Data were merged in R by X-Y coordinates so that each cell could be
542 assessed for all markers simultaneously. Nearest neighbor analysis was performed with
543 the spatstat R package (v1.58-2).

544

545 **Imaging mass cytometry (IMC)**

546 IMC was performed on a 5 μ m section of the same TMA described above. The section
547 was baked at 60°C for 90 min on a hot plate, de-waxed for 20 min in xylene and
548 rehydrated in a graded series of alcohol (100%, 95%, 80% and 70%) for 5 min each.
549 Heat-induced antigen retrieval was conducted on a hot plate at 95°C in Tris-EDTA
550 buffer at pH 9 for 30 min. After blocking with 3% BSA in PBS for 45 min, the section
551 was incubated overnight at 4C with a cocktail of 35 antibodies tagged with rare
552 lanthanide isotopes (**Supplementary Table 5**). The section was counterstained the next
553 day for 40 min with iridium (Ir) and 3 min with ruthenium tetroxide (RuO₄) as
554 described in Catena et al(49). Slides were imaged using the Fluidigm Hyperion IMC
555 system with a 1 μ m laser ablation spot size and frequency of 100-200Hz. A tissue area
556 of 1000 μ m² per sample was ablated and imaged. Duplicate cores of the same samples

557 were ablated when morphologic heterogeneity was identified a priori on H&E.
558 IMCTools (<https://github.com/BodenmillerGroup/imctools>) was used in conjunction
559 with CellProfiler (v2.2.0) to segment images and identify cell objects (see
560 **Supplementary Methods** for details).

561

562 **Cell lines**

563 The cHL cell lines KMH2, L428 and L-1236 were obtained from the German
564 Collection of Microorganisms and Cell Cultures (DSMZ; <http://www.dsmz.de/>)
565 between 2007 and 2010, and were used for experiments within 20 passages. Cultures
566 were grown according to the standard conditions. Human DLBCL cell lines Karpas-422
567 were purchased from DSMZ, and maintained in RPMI1640 (Life Technologies)
568 containing 20% FBS. The cell line OCI-Ly1 was obtained from Dr. L. Staudt (NIH) in
569 2009 and maintained in RPMI1640 (Life Technologies) containing 10% FBS. All cell
570 lines were confirmed negative for *Mycoplasma* prior to culture using the VenorTM GeM
571 Mycoplasma Detection Kit, PCR-based (Sigma-Aldrich, MP0025). All cell lines were
572 authenticated using short tandem repeat profiling.

573

574 **Cell isolation and purification of human T cells**

575 We purified CD4⁺ and CD8⁺ T lymphocytes from peripheral blood mononuclear cells
576 (PBMCs) (see **Supplementary Methods** for details). Isolated CD4⁺ and CD8⁺ T cells
577 were incubated in either supernatants from cHL cell lines (L-1236, L-428, KM-H2) or
578 diffuse large B-cell lymphoma cell lines (OCI-Ly1 and Karpas-422) or culture medium.
579 At the end of day 14, we washed and analyzed the T cells using flow cytometry for
580 characterization. We purified CD4⁺LAG3⁺ T-cells and CD4⁺LAG3⁻ T-cells by flow
581 sorting on a FACS Fusion (BD Biosciences) using a 85µm nozzle.

582

583 **Flow cytometry**

584 To characterize T cells *in vitro*, we stained cells with a panel of antibodies including
585 CD3, CD4, CD8 and LAG3 (see **Supplementary Methods** for details), and assessed
586 them using flow cytometry (LSRFortessa or FACSymphony, BD, Franklin Lakes, NJ,
587 USA). Flow cytometry data were analyzed using FlowJo software (v10.2; TreeStar,
588 Ashland, OR, USA) (**Supplementary Fig. 18**). Statistical analyses were performed
589 using GraphPad Prism Version 7 (GraphPad Software Inc., La Jolla, CA).

590

591 ***In vitro* suppression assay**

592 To evaluate the suppressive activity of LAG3⁺ T cells, we stained CD4⁺ T cells
593 (responder cells) with proliferation dye (VPD450; BD Biosciences or Cell Trace Violet
594 Cell proliferation kit; ThermoFisher) and activated them using soluble monoclonal
595 antibodies to CD3 and CD28 in PRIME XV T cell CDM medium or CD3/CD28 Beads
596 (Thermo Fisher). We added purified CD4⁺ LAG3⁺ T cells induced by cHL cell line
597 supernatant transfer, or purified from cell suspensions of cHL clinical samples
598 (suppressor cells) at a ratio of 1:1. We calculated the percentage of divided responder T
599 cells by gating on CD4⁺ cells and T cell proliferation was determined based on
600 proliferation dye dilution using flow cytometry (LSRFortessa and FACSymphony, BD,
601 Franklin Lakes, NJ, USA).

602

603 **Cytokine and chemokine detection**

604 Cytokines and chemokines were measured by ELISA and custom Bio-Plex assays (see

605 **Supplementary Methods** for details).

606

607 **Generation of *CIITA* knock-out cells**

608 L-428 cell lines were transduced with lentivirus expressing guide sequence against
609 *CIITA* to generate *CIITA* knock-out cells which abrogate the expression of MHC class II
610 (**Supplementary Fig. 19A-B**; see **Supplementary Methods** for details). MHC class II
611 expression was evaluated by staining the cells with FITC-HLA DR/DP/DQ antibody
612 (1:100, BD Biosciences #555558) and analyzed using the BD LSRFortessa™.
613 Subsequently, *CIITA* knock-out cells were sorted by mCherry⁺, HLA DR⁻/DP⁻/DQ⁻,
614 DAPI⁻ using the BD FACSAria™ Fusion sorter.

615

616 ***In vitro* HRS cells and T cell co-culture assay**

617 We purified CD4⁺LAG3⁺ T cells from HLA-class-II matched (to L-428) PBMC as
618 described above. CD4⁺LAG3⁺ T cells were co-cultured with either *CIITA* wild-type or
619 *CIITA* KO L-428 at 2:1 ratio in a 96 well plate.

620

621 **Survival analysis**

622 Overall survival (OS, death from any cause), disease specific survival (DSS, the time
623 from initial diagnosis to death from lymphoma or its treatment, with data for patients

624 who died of unrelated causes censored at the time of death) and post-BMT failure free
625 survival (post-BMT-FFS, time from ASCT treatment to cHL progression, or death from
626 cHL) were analyzed using the Kaplan-Meier method and results were compared using
627 the log rank test. Univariate and multivariate Cox regression analyses were performed
628 to assess the effects of prognostic factors. Survival analyses were performed in the R
629 statistical environment (v3.5.2).

630

631 **Statistical results & visualization**

632 All t-tests reported are two-sided Student's t-tests, and P-values < 0.05 were considered
633 to be statistically significant. In all boxplots, boxes represent the interquartile range with
634 a horizontal line indicating the median value. Whiskers extend to the farthest data point
635 within a maximum of $1.5 \times$ the interquartile range, and colored dots represent outliers.

636

637 **Data availability**

638 Single cell RNA-seq BAM files (generated with CellRanger v2.1.0) are deposited in
639 EGA (EGAS00001004085) and are available by request. The figures associated with
640 the above raw datasets are Fig. 1-4 and Supplementary Fig. 1-10.

641

642 **Code availability**

643 Scripts used for data analysis are available upon request.

644

645 **ACKNOWLEDGEMENTS**

646 This study was funded by a research grant from the CCSRI and a Paul Allen
647 Distinguished Investigator award (Frontiers Group) (C. Steidl). This study was also
648 supported by a Program Project Grant from the Terry Fox Research Institute (C. Steidl,
649 Grant No. 1061), Genome Canada, Genome British Columbia, CIHR, and the British
650 Columbia Cancer Foundation (BCCF). T.A. was supported by fellowship from Japanese
651 Society for The Promotion of Science and the Uehara Memorial Foundation. T.A.
652 received research funding support from The Kanae Foundation for the Promotion of
653 Medical Science. E.V. is supported by a Michael Smith Foundation for Health Research
654 trainee award.

655

656 **AUTHORS' CONTRIBUTIONS**

657 Study design: T.A., L.C., A.M., S.P.S. and C.S.; Writing: T.A., L.C. and C.S.;

658 Manuscript review: K.T., A.M., K.M., M.H., A.C., E.C., T.M-T., V.L., A.W.Z., A.P.W.,
659 K.J.S., D.W.S., G.K., B.N., A.M. and S.P.S.; Data interpretation: T.A., L.C., K.T., M.H.,
660 A.C. and C.S.; *In vitro* experiments: T.A., E.V., B.W.W., A.T., S.H., M.Y.L., X.W.,
661 M.N., J.K. and V.L.; Data analysis: T.A., L.C., M.H., A.C. and K.M.; Single cell
662 processing: E.C.; IHC work: K.T., T.M-T., K.M., P.F., C.G., D.K. and T.G.;

663 Pathological review: K.T., T.M-T. and P.F.; Case identification: T.A., X.W. and A.M.;

664 IMC work: M.H. and A.C.; Supervision: A.P.W., K.J.S., D.W.S., G.K., B.N., A.M.,

665 S.P.S. and C.S.

666

667

668

669

670 **REFERENCES**

- 671 1. Swerdlow SH, Campo E, Harris NL, Jaffe ES, Pileri SA, Stein H., *et al.* WHO
672 Classification of Tumours of Haematopoietic and Lymphoid Tissues. Revised
673 4th ed. Lyon, France: International Agency for Research on Cancer (IARC).
674 2017.
- 675 2. Mottok A, Steidl C. Biology of classical Hodgkin lymphoma: implications for
676 prognosis and novel therapies. *Blood* **2018**;131:1654-65
- 677 3. Aoki T, Steidl C. Novel Biomarker Approaches in Classic Hodgkin Lymphoma.
678 *Cancer J* **2018**;24:206-14
- 679 4. Chan FC, Mottok A, Gerrie AS, Power M, Nijland M, Diepstra A, *et al.*
680 Prognostic Model to Predict Post-Autologous Stem-Cell Transplantation
681 Outcomes in Classical Hodgkin Lymphoma. *J Clin Oncol* **2017**;35:3722-33
- 682 5. Steidl C, Shah SP, Woolcock BW, Rui L, Kawahara M, Farinha P, *et al.* MHC
683 class II transactivator CIITA is a recurrent gene fusion partner in lymphoid
684 cancers. *Nature* **2011**;471:377-81
- 685 6. Steidl C, Lee T, Shah SP, Farinha P, Han G, Nayar T, *et al.* Tumor-associated
686 macrophages and survival in classic Hodgkin's lymphoma. *N Engl J Med*
687 **2010**;362:875-85
- 688 7. Chen R, Zinzani PL, Fanale MA, Armand P, Johnson NA, Brice P, *et al.* Phase
689 II Study of the Efficacy and Safety of Pembrolizumab for Relapsed/Refractory
690 Classic Hodgkin Lymphoma. *J Clin Oncol* **2017**;35:2125-32
- 691 8. Armand P, Engert A, Younes A, Fanale M, Santoro A, Zinzani PL, *et al.*
692 Nivolumab for Relapsed/Refractory Classic Hodgkin Lymphoma After Failure
693 of Autologous Hematopoietic Cell Transplantation: Extended Follow-Up of the
694 Multicohort Single-Arm Phase II CheckMate 205 Trial. *J Clin Oncol*
695 **2018**;36:1428-39
- 696 9. Younes A, Gopal AK, Smith SE, Ansell SM, Rosenblatt JD, Savage KJ, *et al.*
697 Results of a pivotal phase II study of brentuximab vedotin for patients with
698 relapsed or refractory Hodgkin's lymphoma. *J Clin Oncol* **2012**;30:2183-9
- 699 10. Cader FZ, Schackmann RCJ, Hu X, Wienand K, Redd R, Chapuy B, *et al.* Mass
700 cytometry of Hodgkin lymphoma reveals a CD4(+) regulatory T-cell-rich and
701 exhausted T-effector microenvironment. *Blood* **2018**;132:825-36

- 702 11. Greaves P, Clear A, Owen A, Iqbal S, Lee A, Matthews J, *et al.* Defining
703 characteristics of classical Hodgkin lymphoma microenvironment T-helper cells.
704 *Blood* **2013**;122:2856-63
- 705 12. Patel SS, Weirather JL, Lipschitz M, Lako A, Chen PH, Griffin GK, *et al.* The
706 microenvironmental niche in classic Hodgkin lymphoma is enriched for
707 CTLA-4- positive T-cells that are PD-1-negative. *Blood* **2019** Oct 10. E-pub
708 ahead of print
- 709 13. Azizi E, Carr AJ, Plitas G, Cornish AE, Konopacki C, Prabhakaran S, *et al.*
710 Single-Cell Map of Diverse Immune Phenotypes in the Breast Tumor
711 Microenvironment. *Cell* **2018**;174:1293-308 e36
- 712 14. Han A, Glanville J, Hansmann L, Davis MM. Linking T-cell receptor sequence
713 to functional phenotype at the single-cell level. *Nat Biotechnol* **2014**;32:684-92
- 714 15. Zilionis R, Nainys J, Veres A, Savova V, Zemmour D, Klein AM, *et al.*
715 Single-cell barcoding and sequencing using droplet microfluidics. *Nat Protoc*
716 **2017**;12:44-73
- 717 16. Klein AM, Mazutis L, Akartuna I, Tallapragada N, Veres A, Li V, *et al.* Droplet
718 barcoding for single-cell transcriptomics applied to embryonic stem cells. *Cell*
719 **2015**;161:1187-201
- 720 17. Novershtern N, Subramanian A, Lawton LN, Mak RH, Haining WN, McConkey
721 ME, *et al.* Densely interconnected transcriptional circuits control cell states in
722 human hematopoiesis. *Cell* **2011**;144:296-309
- 723 18. Netea MG, Azam T, Ferwerda G, Girardin SE, Walsh M, Park JS, *et al.* IL-32
724 synergizes with nucleotide oligomerization domain (NOD) 1 and NOD2 ligands
725 for IL-1beta and IL-6 production through a caspase 1-dependent mechanism.
726 *Proc Natl Acad Sci U S A* **2005**;102:16309-14
- 727 19. Schmitz R, Stanelle J, Hansmann ML, Kuppers R. Pathogenesis of classical and
728 lymphocyte-predominant Hodgkin lymphoma. *Annu Rev Pathol* **2009**;4:151-74
- 729 20. Morales O, Mrizak D, Francois V, Mustapha R, Miroux C, Depil S, *et al.*
730 Epstein-Barr virus infection induces an increase of T regulatory type 1 cells in
731 Hodgkin lymphoma patients. *Br J Haematol* **2014**;166:875-90
- 732 21. Gandhi MK, Lambley E, Duraiswamy J, Dua U, Smith C, Elliott S, *et al.*
733 Expression of LAG-3 by tumor-infiltrating lymphocytes is coincident with the
734 suppression of latent membrane antigen-specific CD8+ T-cell function in
735 Hodgkin lymphoma patients. *Blood* **2006**;108:2280-9

- 736 22. Gagliani N, Magnani CF, Huber S, Gianolini ME, Pala M, Licona-Limon P, *et al.*
737 *al.* Coexpression of CD49b and LAG-3 identifies human and mouse T
738 regulatory type 1 cells. *Nat Med* **2013**;19:739-46
- 739 23. Andrews LP, Marciscano AE, Drake CG, Vignali DA. LAG3 (CD223) as a
740 cancer immunotherapy target. *Immunol Rev* **2017**;276:80-96
- 741 24. Tumeh PC, Harview CL, Yearley JH, Shintaku IP, Taylor EJ, Robert L, *et al.*
742 PD-1 blockade induces responses by inhibiting adaptive immune resistance.
743 *Nature* **2014**;515:568-71
- 744 25. Haghverdi L, Buettner F, Theis FJ. Diffusion maps for high-dimensional
745 single-cell analysis of differentiation data. *Bioinformatics* **2015**;31:2989-98
- 746 26. Coifman RR, Lafon S, Lee AB, Maggioni M, Nadler B, Warner F, *et al.*
747 Geometric diffusions as a tool for harmonic analysis and structure definition of
748 data: diffusion maps. *Proc Natl Acad Sci U S A* **2005**;102:7426-31
- 749 27. Huang CT, Workman CJ, Flies D, Pan X, Marson AL, Zhou G, *et al.* Role of
750 LAG-3 in regulatory T cells. *Immunity* **2004**;21:503-13
- 751 28. Bacchetta R, Sartirana C, Levings MK, Bordignon C, Narula S, Roncarolo MG.
752 Growth and expansion of human T regulatory type 1 cells are independent from
753 TCR activation but require exogenous cytokines. *Eur J Immunol*
754 **2002**;32:2237-45
- 755 29. Groux H, O'Garra A, Bigler M, Rouleau M, Antonenko S, de Vries JE, *et al.* A
756 CD4⁺ T-cell subset inhibits antigen-specific T-cell responses and prevents
757 colitis. *Nature* **1997**;389:737-42
- 758 30. Skinnider BF, Mak TW. The role of cytokines in classical Hodgkin lymphoma.
759 *Blood* **2002**;99:4283-97
- 760 31. Lin Y, Xu L, Jin H, Zhong Y, Di J, Lin QD. CXCL12 enhances exogenous
761 CD4⁺CD25⁺ T cell migration and prevents embryo loss in non-obese diabetic
762 mice. *Fertil Steril* **2009**;91:2687-96
- 763 32. McFadden C, Morgan R, Rahangdale S, Green D, Yamasaki H, Center D, *et al.*
764 Preferential migration of T regulatory cells induced by IL-16. *J Immunol*
765 **2007**;179:6439-45
- 766 33. Wang X, Lang M, Zhao T, Feng X, Zheng C, Huang C, *et al.* Cancer-FOXP3
767 directly activated CCL5 to recruit FOXP3(+)Treg cells in pancreatic ductal
768 adenocarcinoma. *Oncogene* **2017**;36:3048-58

- 769 34. Pierini A, Strober W, Moffett C, Baker J, Nishikii H, Alvarez M, *et al.*
770 TNF-alpha priming enhances CD4+FoxP3+ regulatory T-cell suppressive
771 function in murine GVHD prevention and treatment. *Blood* **2016**;128:866-71
- 772 35. Tran DQ. TGF-beta: the sword, the wand, and the shield of FOXP3(+)
773 regulatory T cells. *J Mol Cell Biol* **2012**;4:29-37
- 774 36. Gobert M, Treilleux I, Bendriss-Vermare N, Bachelot T, Goddard-Leon S, Arfi
775 V, *et al.* Regulatory T cells recruited through CCL22/CCR4 are selectively
776 activated in lymphoid infiltrates surrounding primary breast tumors and lead to
777 an adverse clinical outcome. *Cancer Res* **2009**;69:2000-9
- 778 37. Mizukami Y, Kono K, Kawaguchi Y, Akaike H, Kamimura K, Sugai H, *et al.*
779 CCL17 and CCL22 chemokines within tumor microenvironment are related to
780 accumulation of Foxp3+ regulatory T cells in gastric cancer. *Int J Cancer*
781 **2008**;122:2286-93
- 782 38. Jin JO, Han X, Yu Q. Interleukin-6 induces the generation of IL-10-producing
783 Tr1 cells and suppresses autoimmune tissue inflammation. *J Autoimmun*
784 **2013**;40:28-44
- 785 39. Steidl C, Diepstra A, Lee T, Chan FC, Farinha P, Tan K, *et al.* Gene expression
786 profiling of microdissected Hodgkin Reed-Sternberg cells correlates with
787 treatment outcome in classical Hodgkin lymphoma. *Blood* **2012**;120:3530-40
- 788 40. Huard B, Prigent P, Pages F, Bruniquel D, Triebel F. T cell major
789 histocompatibility complex class II molecules down-regulate CD4+ T cell clone
790 responses following LAG-3 binding. *Eur J Immunol* **1996**;26:1180-6
- 791 41. Baixeras E, Huard B, Miossec C, Jitsukawa S, Martin M, Hercend T, *et al.*
792 Characterization of the lymphocyte activation gene 3-encoded protein. A new
793 ligand for human leukocyte antigen class II antigens. *J Exp Med*
794 **1992**;176:327-37
- 795 42. Duffield AS, Ascierto ML, Anders RA, Taube JM, Meeker AK, Chen S, *et al.*
796 Th17 immune microenvironment in Epstein-Barr virus-negative Hodgkin
797 lymphoma: implications for immunotherapy. *Blood Adv* **2017**;1:1324-34
- 798 43. Roemer MGM, Redd RA, Cader FZ, Pak CJ, Abdelrahman S, Ouyang J, *et al.*
799 Major Histocompatibility Complex Class II and Programmed Death Ligand 1
800 Expression Predict Outcome After Programmed Death 1 Blockade in Classic
801 Hodgkin Lymphoma. *J Clin Oncol* **2018**;36:942-50

- 802 44. Zhang B, Chikuma S, Hori S, Fagarasan S, Honjo T. Nonoverlapping roles of
803 PD-1 and FoxP3 in maintaining immune tolerance in a novel autoimmune
804 pancreatitis mouse model. *Proc Natl Acad Sci U S A* **2016**;113:8490-5
- 805 45. Wang J, Sanmamed MF, Datar I, Su TT, Ji L, Sun J, *et al.* Fibrinogen-like
806 Protein 1 Is a Major Immune Inhibitory Ligand of LAG-3. *Cell*
807 **2019**;176:334-47 e12
- 808 46. Xu F, Liu J, Liu D, Liu B, Wang M, Hu Z, *et al.* LSECtin expressed on
809 melanoma cells promotes tumor progression by inhibiting antitumor T-cell
810 responses. *Cancer Res* **2014**;74:3418-28
- 811 47. Lun AT, Bach K, Marioni JC. Pooling across cells to normalize single-cell RNA
812 sequencing data with many zero counts. *Genome Biol* **2016**;17:75
- 813 48. Levine JH, Simonds EF, Bendall SC, Davis KL, Amir el AD, Tadmor MD, *et al.*
814 Data-Driven Phenotypic Dissection of AML Reveals Progenitor-like Cells that
815 Correlate with Prognosis. *Cell* **2015**;162:184-97
- 816 49. Catena R, Montuenga LM, Bodenmiller B. Ruthenium counterstaining for
817 imaging mass cytometry. *J Pathol* **2018**;244:479-84

818

819

820 **FIGURE LEGENDS**

821 **Figure 1. Immune cell atlas of the Hodgkin lymphoma microenvironment at**
822 **single-cell resolution.** Cells from 22 cHL and 5 RLN cases were clustered using the
823 PhenoGraph algorithm to identify groups of cells with similar expression patterns. **A,**
824 Heatmap summarizing mean expression (normalized and log-transformed) of selected
825 canonical markers in each cluster. Data has been scaled row-wise for visualization. The
826 covariate bar on the left side indicates the component associated with each gene, and
827 black boxes highlight prominent expression of known subtype genes. **B,** Single-cell
828 expression of all cells from cHL and RLN in tSNE space (first two dimensions). Cells
829 are colored according to PhenoGraph cluster. Subsets of cells from cHL and RLN
830 samples are shown on the same coordinates below, respectively. **C,** Proportion of cells
831 in each cluster originating from cHL and RLN samples. Clusters labeled in red highlight
832 Treg clusters. Dashed white line represents the proportion of RLN cells in the total
833 population. **D,** The proportion of cells assigned to a given immune cell type (as
834 determined by cluster) was calculated for each sample. Boxplots summarize the
835 distribution of the proportions for all samples, grouped by tissue type (cHL or RLN).
836 P-values calculated using a t-test are shown above, and demonstrate a significant
837 expansion in the proportion of Tregs present in cHL compared to RLN. **E,** Proportion of

838 CD4⁺ T cells (non-Treg) assigned to various subsets, calculated per sample and
839 summarized with boxplots (see Methods for definition of subtypes). **F-G**, Proportion of
840 immune cell types as in **D-E**, with samples separated according to EBV status (RLN not
841 included). **H**, Proportion of immune cell types as in **e**, with samples separated according
842 to histological subtype (RLN not included).

843

844 **Figure 2. Detailed characterization and co-expression patterns of regulatory T cells**

845 **in the tumor microenvironment of classic Hodgkin Lymphoma. A**, Violin plots

846 showing distribution of expression values (normalized log-transformed) for genes

847 associated with Treg function. Cells from three cluster types are included: CD4⁺ T cells

848 (non-Treg) (CD4-C1-Helper, CD4-C2-Helper and CD4-C3-Helper), LAG3⁺ Tregs

849 (CD4-C5-Treg) and other Tregs (CD4-C4-Treg and CD4-C6-Treg). **B**, The number of

850 individual cells co-expressing Treg markers LAG3 and FOXP3 in all Treg clusters. **C**,

851 Proportion of LAG3 and PDCD1 (PD-1) positive cells in each cluster. **D**, Proportion of

852 LAG3 and PD-1 positive cells in all Tregs, CD4⁺ T cells (non-Tregs), and all CD8⁺ T

853 cells. **E**, Heatmap showing mean expression of inhibitory receptors for cluster subsets.

854 Expression values have been scaled row-wise for visualization. **F**, UpSet plot showing

855 co-expression patterns of inhibitory receptors (LAG3, PD-1, TIGIT, TIM3 and CTLA4)
856 for individual cells in the LAG3⁺ Treg cluster. **G**, Cellular trajectories were inferred
857 using diffusion map analysis of cells in all CD4⁺ T cell clusters (cHL cells only).
858 Individual cells are shown in the first two resulting dimensions, and are colored
859 according to cluster (LAG3⁺ Treg cluster is shown in bold). Axis labels indicate the
860 signature most correlated with each dimension (see Methods).

861

862 **Figure 3. An immune suppressive microenvironment is characteristic of cHL and**

863 **is associated with LAG3 positivity.** **A**, Density plots showing the expression of
864 suppressive cytokines for cells in the LAG3⁺ Treg cluster (CD4-C5-Treg). Cells are
865 grouped by LAG3 positivity and P-values were calculated using t-tests. **B**,

866 Representative flow cytometric analysis of CD25 and LAG3 expression on T cells
867 isolated from PBMCs cultured with supernatant of cHL cell line, L-1236, or medium,
868 respectively. **C**, The proportion of LAG3⁺ cells among CD4⁺ T cells cultured with

869 supernatant of cHL cell lines (KM-H2, L-428 and L-1236), diffuse large B-cell
870 lymphoma (DLBCL) cell lines (OCI-Ly1 and Karpas-422) or medium only. Data are
871 shown as the mean±SEM (n = 3). *P ≤ 0.05; **P ≤ 0.01. **D**, The amount of cytokines

872 and chemokines in the supernatant of cHL cell lines and DLBCL cell lines by Luminex

873 analysis. Data are shown as the mean \pm SEM (n = 3). **E**, The amount of cytokines and
874 chemokines in the supernatant of FACS-sorted CD4⁺LAG3⁺ cells and CD4⁺LAG3⁻
875 cells by Luminex analysis. Data are shown as the mean \pm SEM (n = 4). ****P** \leq 0.01, ***P** \leq
876 0.0001. **F**, (left) A representative experiment showing proliferation of CD4⁺ responder
877 T cells alone (bottom), co-cultured with FACS-sorted CD4⁺LAG⁻ T cells (middle), or
878 co-cultured with FACS-sorted CD4⁺LAG3⁺ T cells (top). (right) The percentage of
879 proliferating CD4⁺ responder T cells in each co-culture condition, relative to the normal
880 proliferation rate (alone). Data are shown as the mean \pm SEM (n = 4). ***P** \leq 0.05.

881

882 **Figure 4. Spatial distribution of Hodgkin and Reed-Sternberg cells and LAG3⁺ T**
883 **cells in cHL tumors. A**, Representative LAG3 immunohistochemistry of cHL tumor
884 biopsies and a reactive lymph node (\times 400, CHL03 and CHL05). **B**, Boxplot showing
885 mean LAG3 expression of cells in the LAG3⁺ Treg cluster separated by MHC class II
886 (MHC-II) status on HRS cells as determined by IHC (P = 0.0186; t-test). **C**, Volcano
887 plot showing differentially expressed genes between cells in the LAG3⁺ Treg cluster
888 originating from MHC-II positive or negative cases. The top 5 genes by absolute log
889 fold-change in each direction are highlighted in red. The y-axis summarizes P-values

890 corrected for multiple testing using the Benjamini-Hochberg method. **D**, IHC staining
891 for major immune cell markers in representative cases with either MHC-II positive HRS
892 cells (left) or MHC-II negative (right) HRS cells ($\times 400$). **E**, Boxplot showing the
893 density of $CD4^+ LAG3^+$ T cells (left) or $CD4^+ FOXP3^+$ (right) in the region surrounding
894 $CD30^+$ cells (HRS) for each sample, separated by tissue type and MHC-II status on HRS
895 cells (t-test; ns: $P > 0.05$, *: $P \leq 0.05$, ***: $P \leq 0.001$, ****: $P \leq 0.0001$). **F**, Average
896 nearest neighbor (NN) distance from an HRS cell ($CD30^+$) to the closest $CD4^+ LAG3^+$
897 cell (left) or $CD4^+ FOXP3^+$ cell (right) was calculated per sample, and separated by
898 MHC-II status on HRS cells. P-values were calculated using t-tests. **G**, Multicolor IF
899 staining (CHL03 and CHL05) for CD30 (yellow), MHC-II (green), and LAG3
900 (magenta) shows localization of $LAG3^+ CD4^+$ T cells to the region surrounding HRS
901 cells in cases with MHC-II negative HRS cells.

902

903 **Figure 5. Co-expression patterns and localization of immune cells according to**
904 **HRS MHC-II status, using imaging mass cytometry.** **A**, A representative case with
905 MHC-II negative cHL case (CHL5) shows numerous $LAG3^+ CD4^+$ T cells (i) and few
906 $FOXP3^+ CD4^+$ T cells (ii), with the $LAG3^+$ cells rosetting the HRS cells (iii-iv). In
907 contrast, a representative MHC-II positive cHL case (CHL3) shows rare $LAG3^+ CD4^+$

908 T cells (v) and abundant FOXP3⁺ CD4⁺ T cells (vi), the latter surrounding HRS cells
909 (vii-viii). **B**, Comparison of the proportion of LAG3⁺ cells by MHC-II status in a
910 validation cohort.(6) P-values were calculated using t-tests. **C**, Comparison of the
911 proportion of LAG3⁺ cells by EBV status in a validation cohort.(6) P-values were
912 calculated using t-tests.

913

914 **Figure 6. Interactions of HRS cells and CD4⁺ LAG3⁺ T cells.** **A**, The expression of
915 cytokines and chemokines on micro-dissected HRS cells from primary HL samples
916 (separated by MHC class II status) and germinal center cells from reactive tonsil (GCB)
917 (t-test; ns: P > 0.05, *: P ≤ 0.05, **: P ≤ 0.01, ****: P ≤ 0.0001). **B**, The proportion of
918 LAG3⁺ cells among CD4⁺ T cells after co-culture with supernatant of cHL cell lines
919 (L-1236), medium with IL-6, or medium only. Data are shown as the mean ± SEM (n =
920 4) (**: P ≤ 0.01). **C**, (left) A representative experiment showing LAG3 expression of
921 CD4⁺LAG3⁺ T cells (HLA-matched with L-428) after co-culture with either *CIITA*
922 wild-type (Red) or *CIITA* KO L-428 (Blue). LAG3 expression on the T cells was
923 significantly decreased after co-culture with MHC-II positive (*CIITA* KO) cells. (right)
924 The percentage of highly-expressing LAG3⁺ T cells after co-culture with L-428 *CIITA*
925 variants (wild-type or knockout). Data are shown as the mean ± SEM (n = 3). *: P ≤

926 0.05. **D**, (left) A representative experiment showing proliferation of CD4⁺ T cells sorted
927 from cHL clinical samples (red), and the same cells co-cultured with CD4⁺LAG3⁺
928 CD25⁺T cells from cHL clinical samples (blue). (right) The percentage of proliferating
929 cells in each condition are shown as the mean \pm SEM (n = 4). *: P \leq 0.05 (t-test). **E**, The
930 expression of TNF α in the populations described in **D** are shown as the mean \pm SEM (n
931 = 3). *: P \leq 0.05 (t-test).

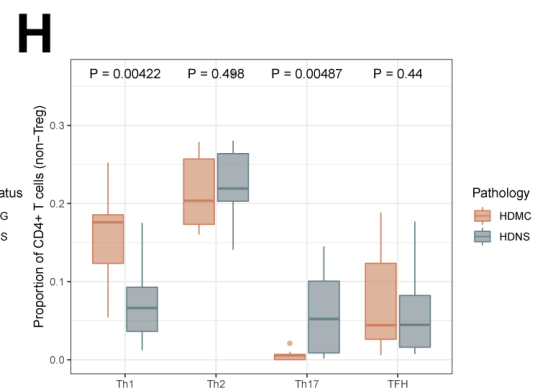
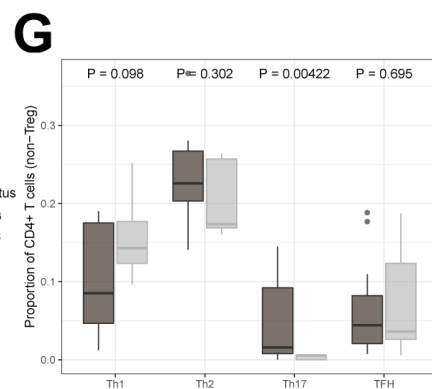
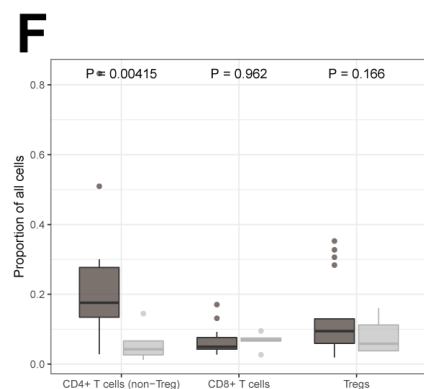
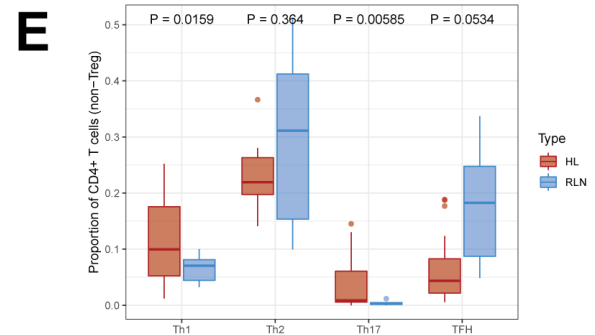
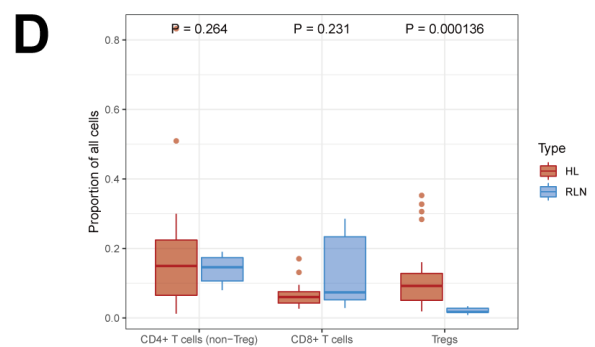
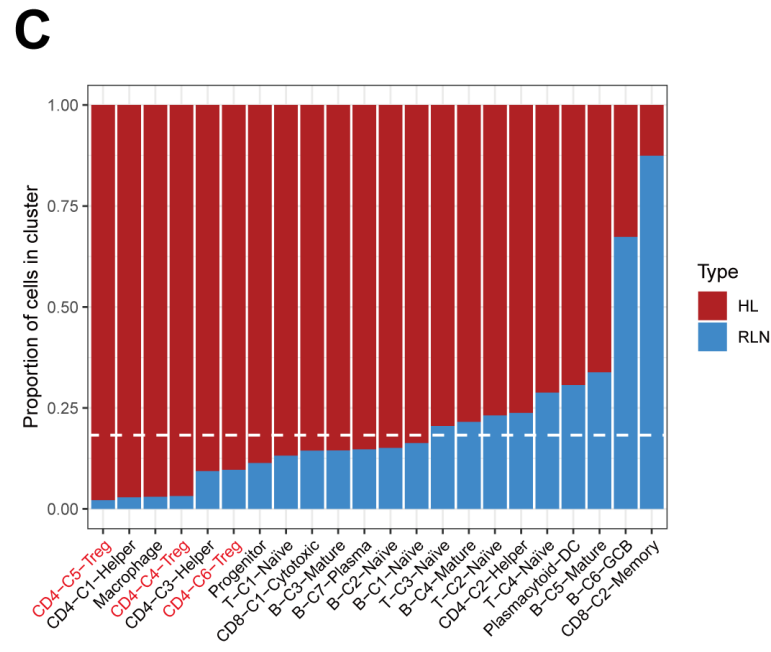
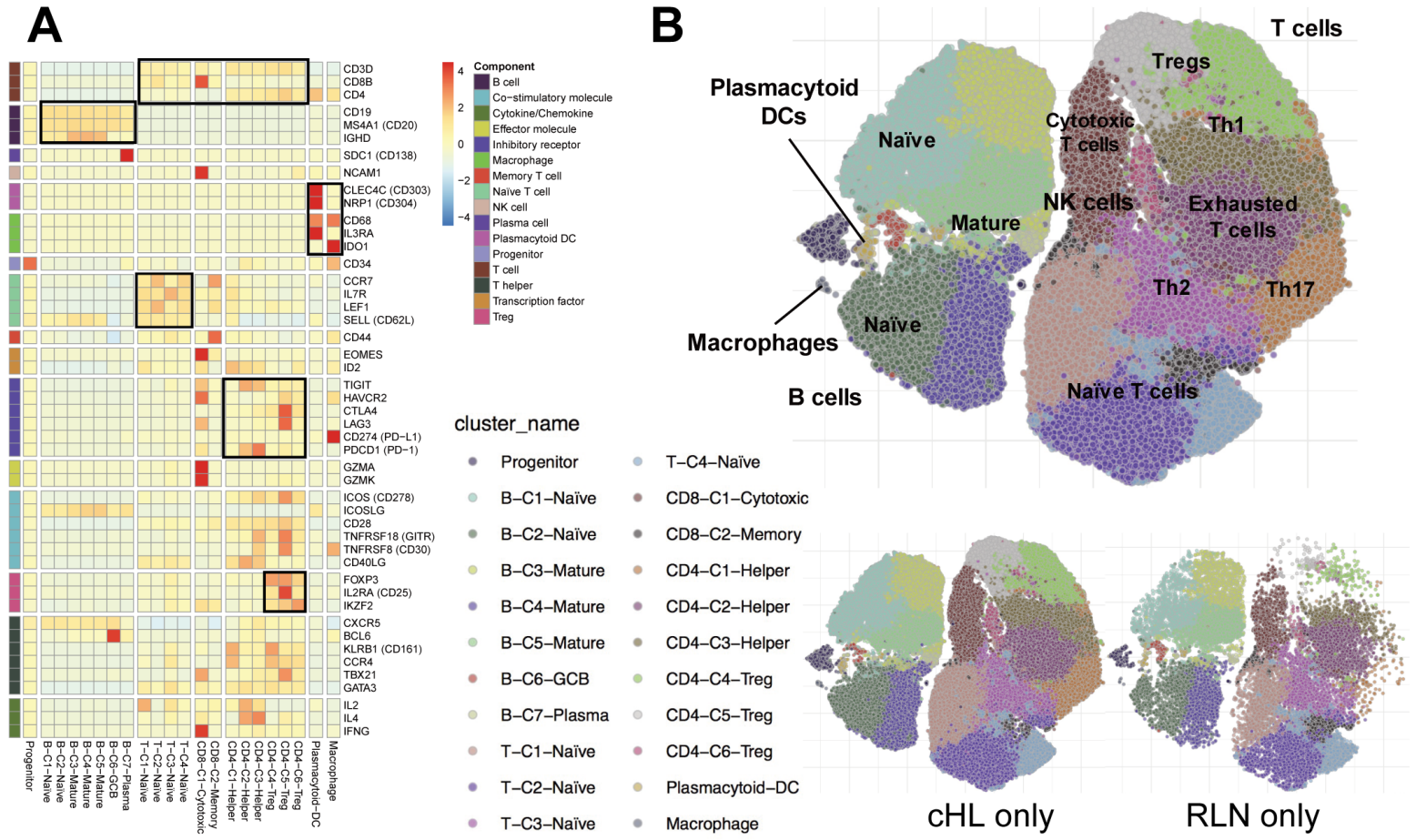
932

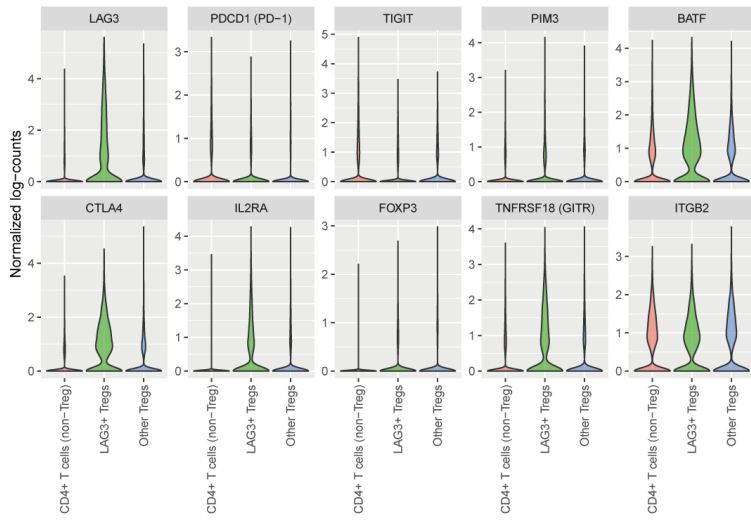
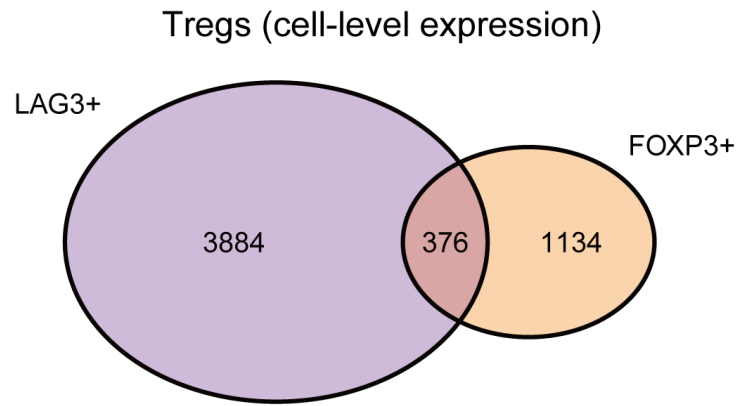
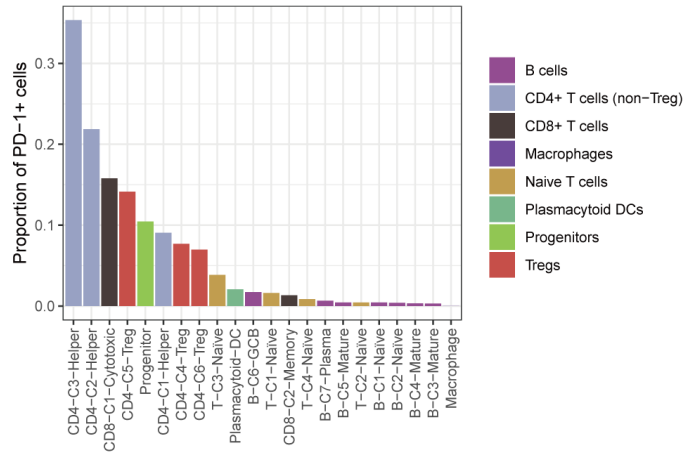
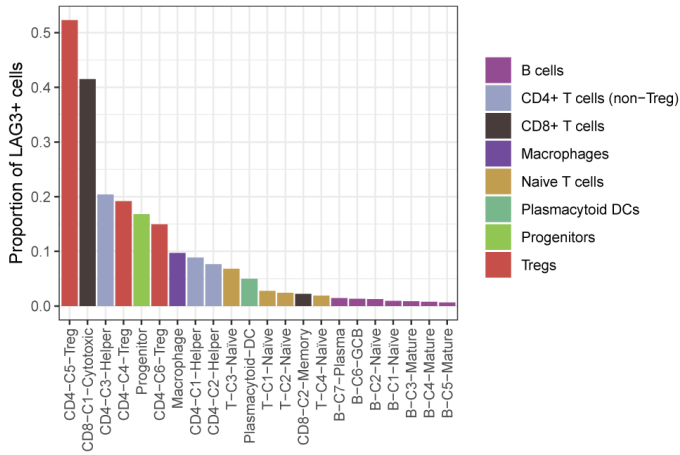
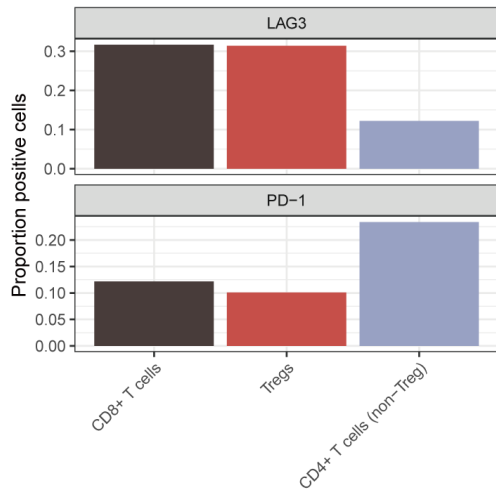
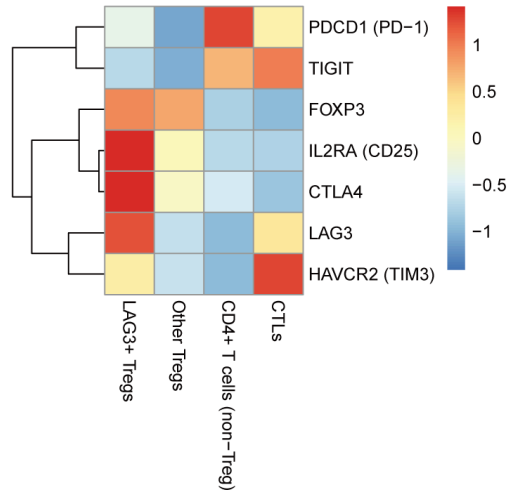
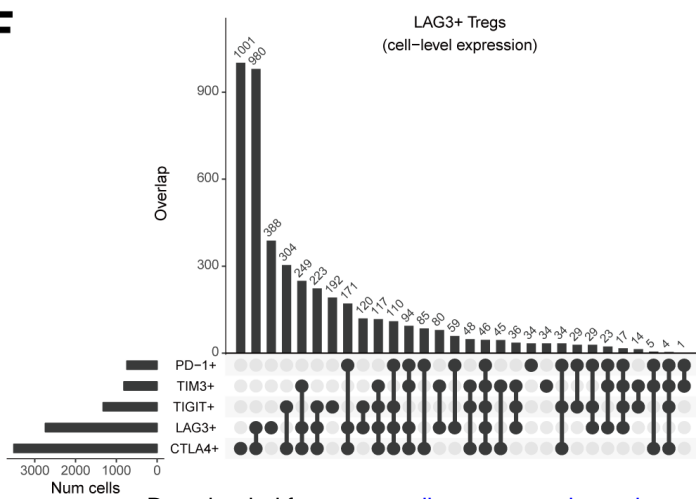
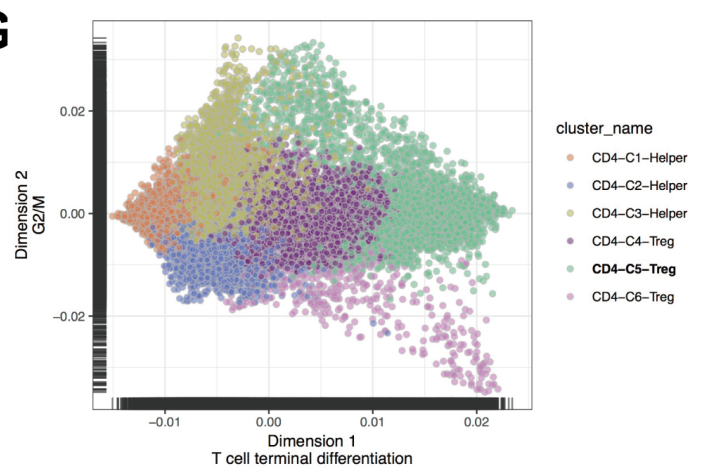
933 **Figure 7. A model of LAG3⁺ T cell and HRS cell interactions in classic Hodgkin**

934 **lymphoma.**

935 Hypothetical model of LAG3⁺ T cell and HRS cell interactions in cHL. MHC-II
936 negative HRS cells (Type 1) secrete cytokines that induce LAG3 in CD4⁺ T cells. CD4⁺
937 LAG3⁺ T cells surround HRS cells and secrete suppressive cytokines. MHC-II positive
938 cells (Type 2) secrete a distinct set of cytokines that attract FOXP3⁺ and Th17 cells.

939



A**B****C****D****E****F****G**

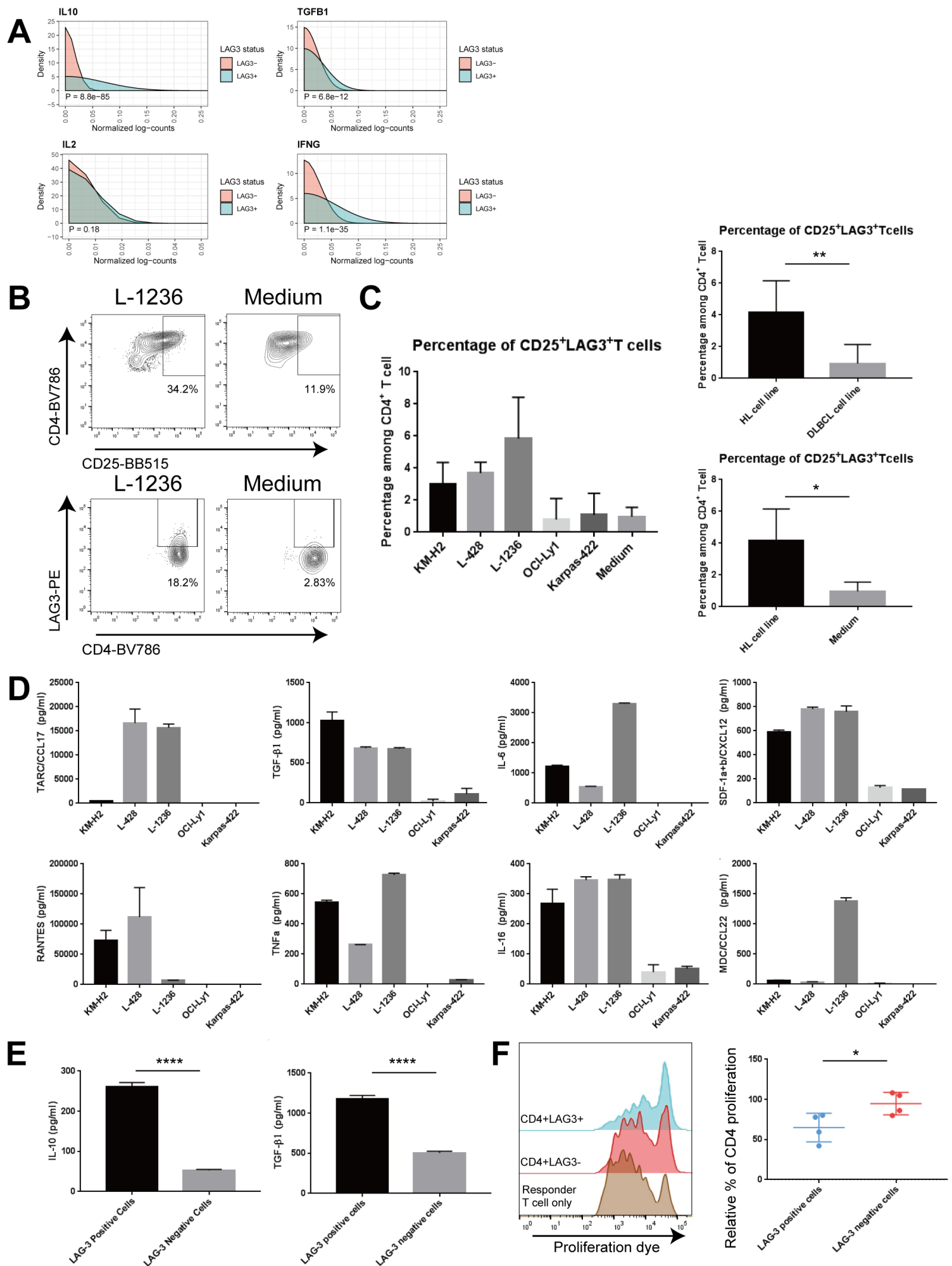
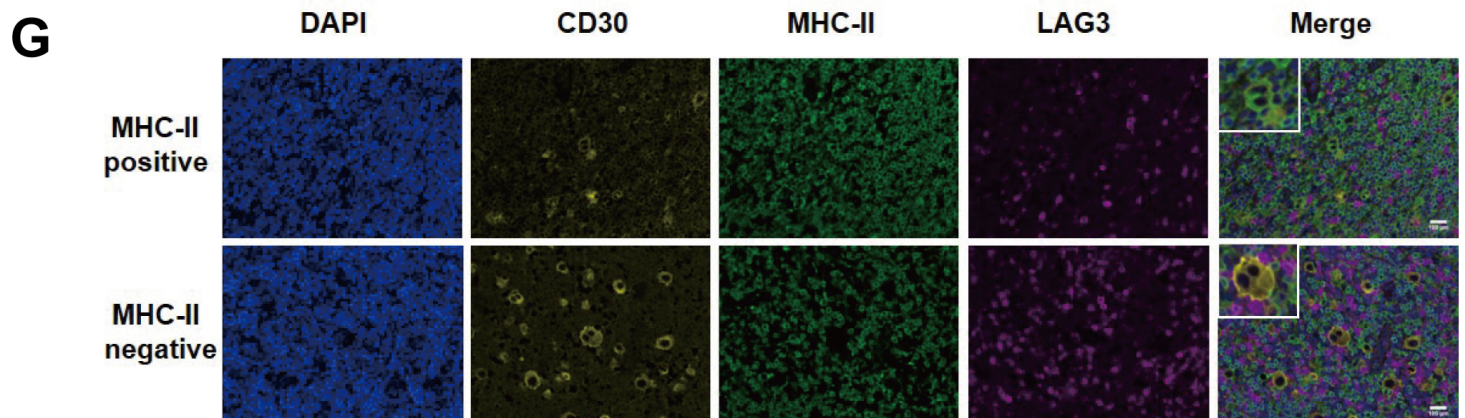
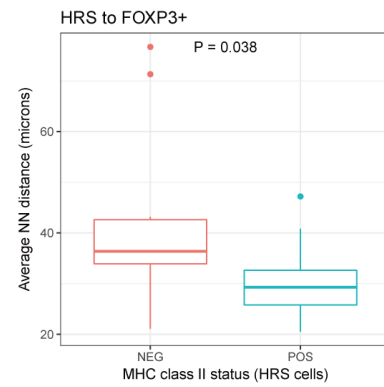
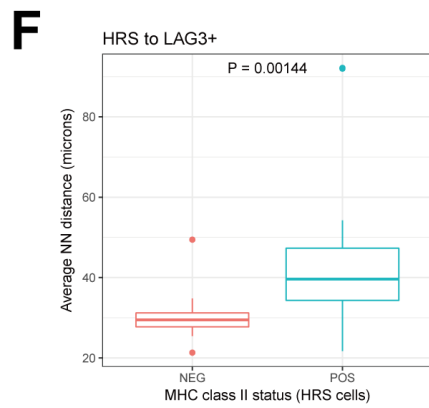
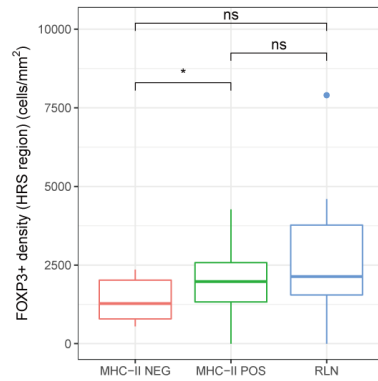
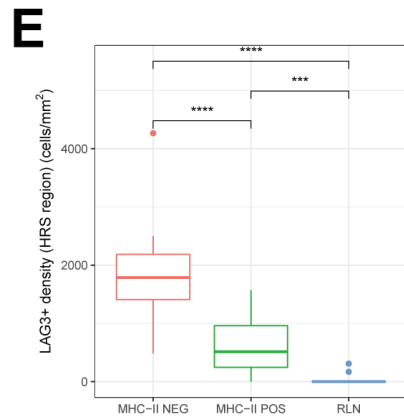
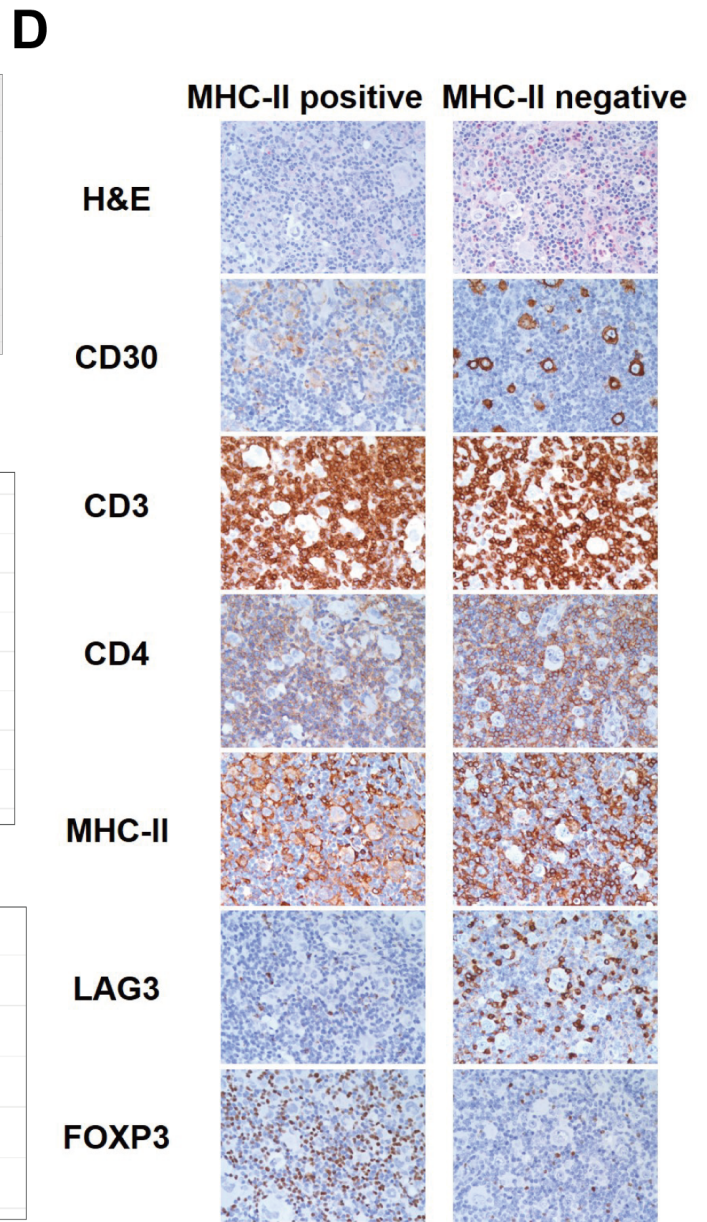
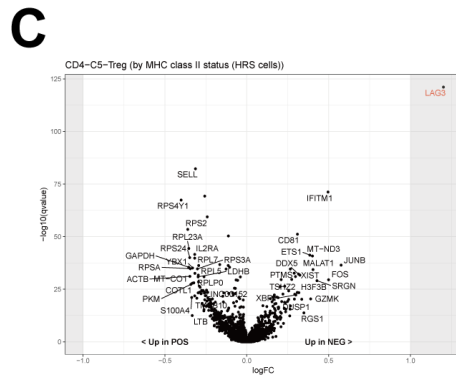
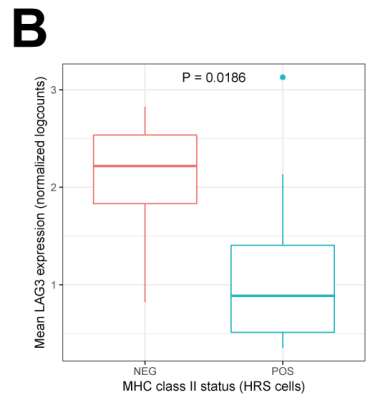
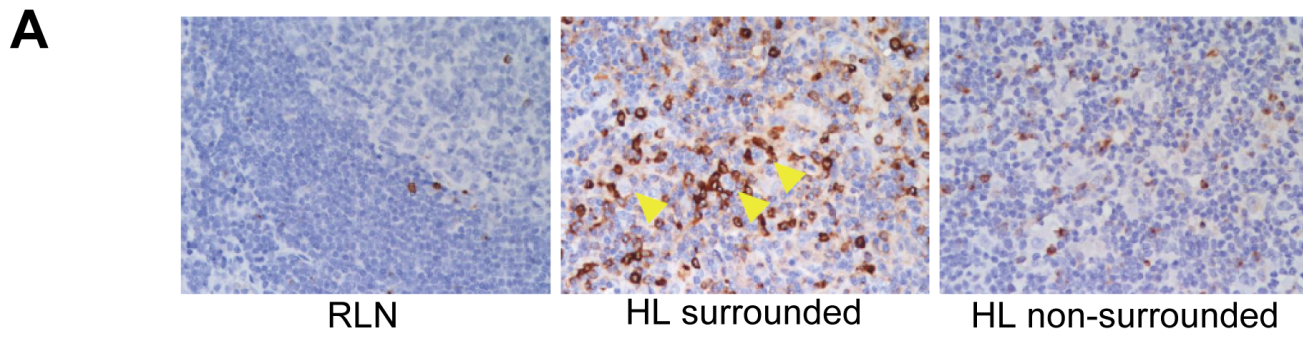


Figure 3
 Downloaded from cancerdiscovery.aacrjournals.org on January 13, 2020. © 2019 American Association for Cancer Research.



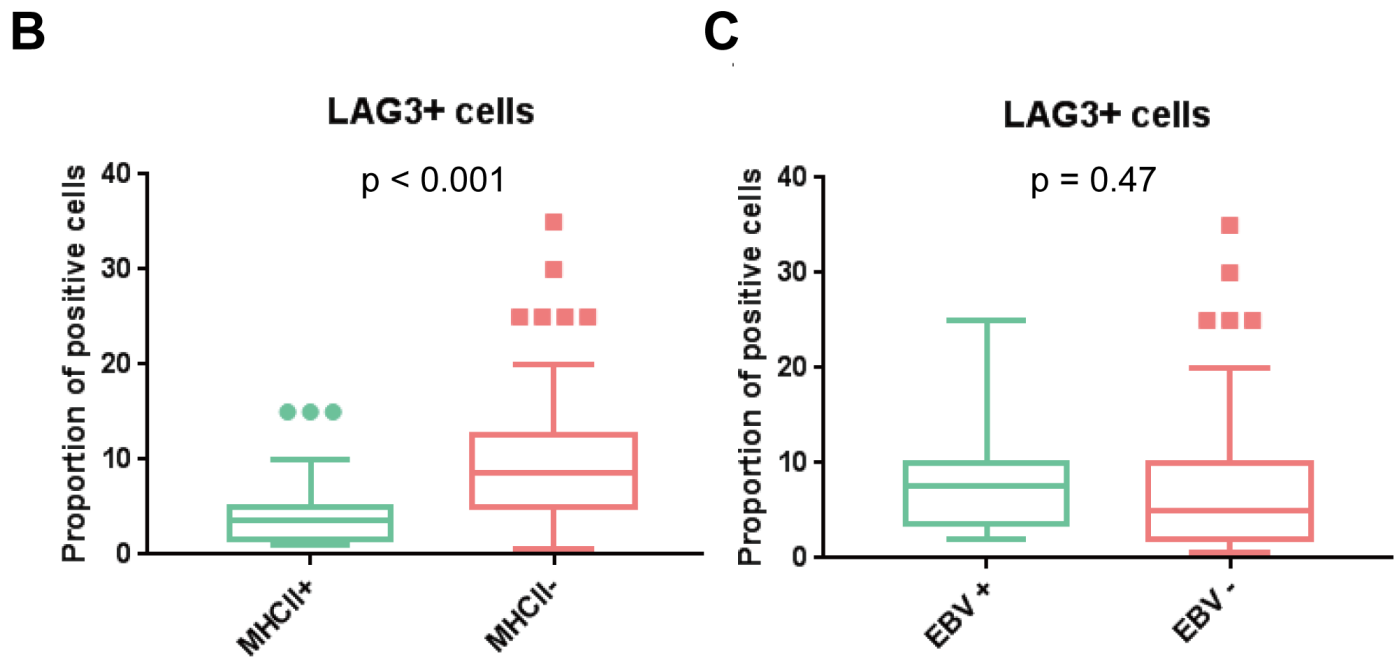
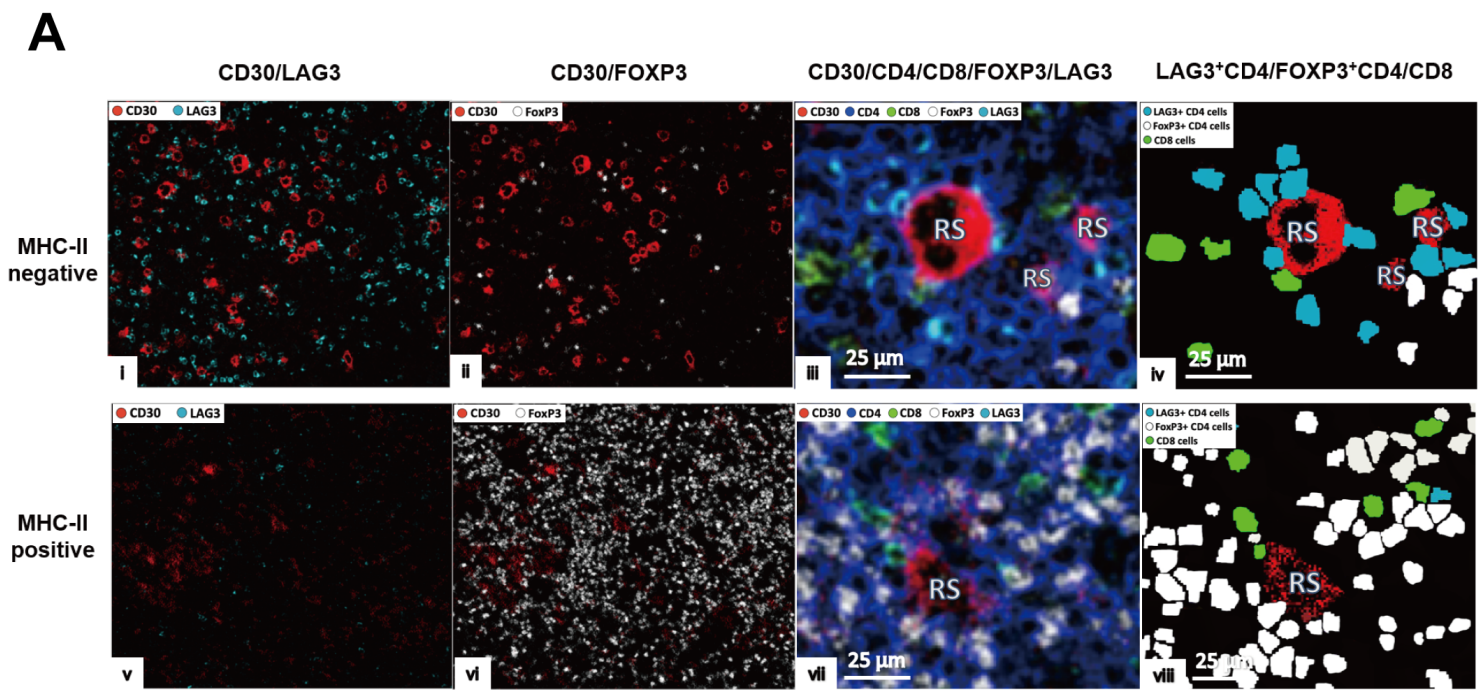


Figure 5

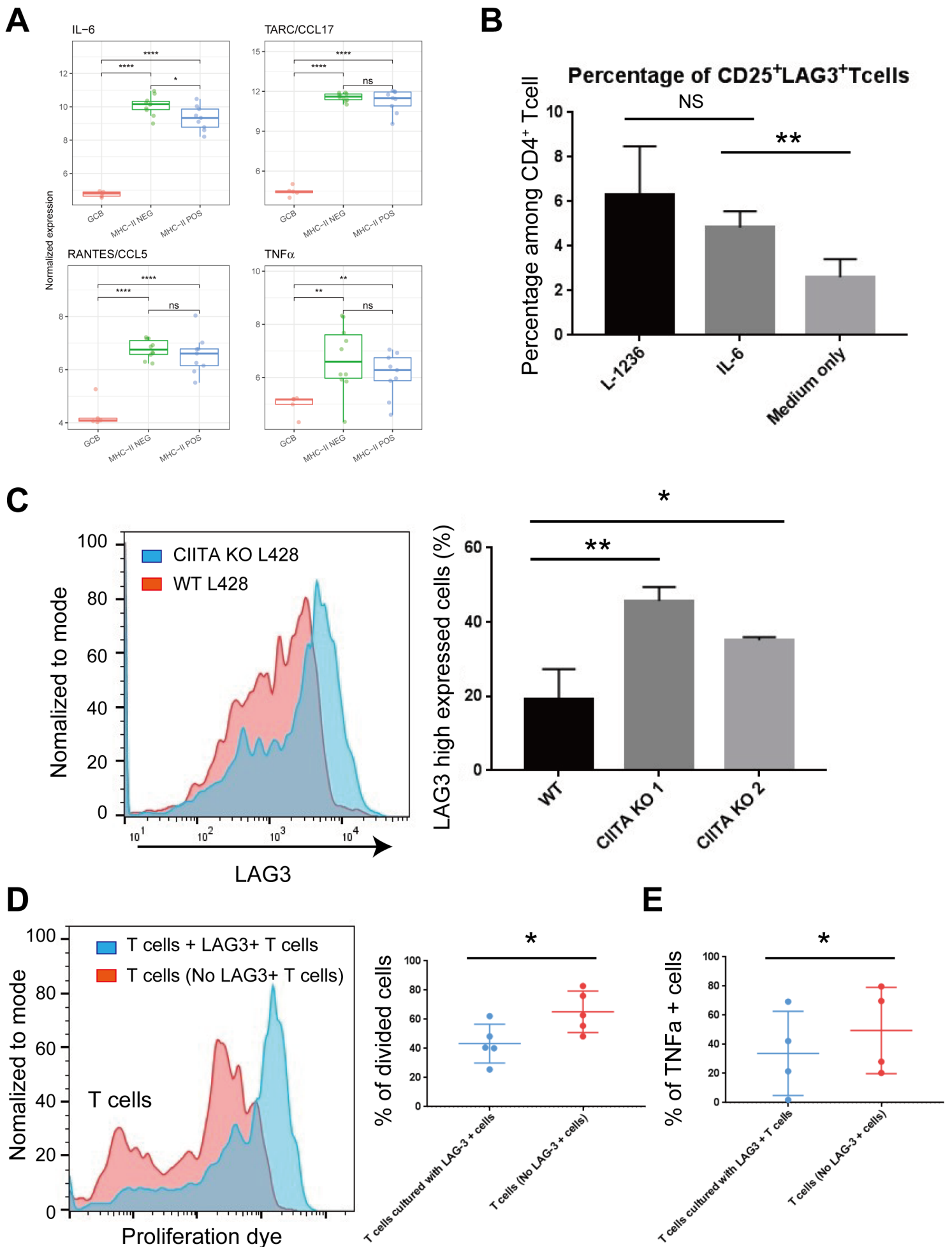


Figure 6

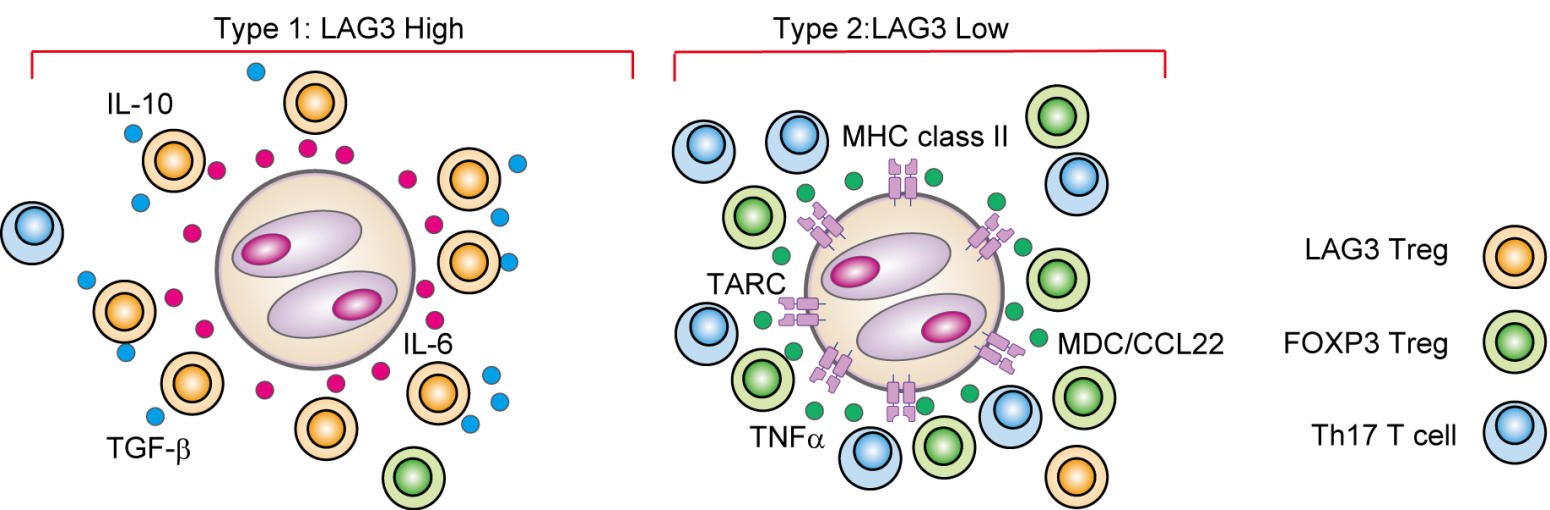


Figure 7

CANCER DISCOVERY

Single cell transcriptome analysis reveals disease-defining T cell subsets in the tumor microenvironment of classic Hodgkin lymphoma

Tomohiro Aoki, Lauren C Chong, Katsuyoshi Takata, et al.

Cancer Discov Published OnlineFirst December 19, 2019.

Updated version	Access the most recent version of this article at: doi: 10.1158/2159-8290.CD-19-0680
Supplementary Material	Access the most recent supplemental material at: http://cancerdiscovery.aacrjournals.org/content/suppl/2019/12/18/2159-8290.CD-19-0680.DC1
Author Manuscript	Author manuscripts have been peer reviewed and accepted for publication but have not yet been edited.

E-mail alerts	Sign up to receive free email-alerts related to this article or journal.
Reprints and Subscriptions	To order reprints of this article or to subscribe to the journal, contact the AACR Publications Department at pubs@aacr.org .
Permissions	To request permission to re-use all or part of this article, use this link http://cancerdiscovery.aacrjournals.org/content/early/2019/12/18/2159-8290.CD-19-0680 . Click on "Request Permissions" which will take you to the Copyright Clearance Center's (CCC) Rightslink site.